LOOP OSCILLATIONS IN THE CORONA

Lorna James

A Thesis Submitted for the Degree of MPhil
at the
University of St Andrews

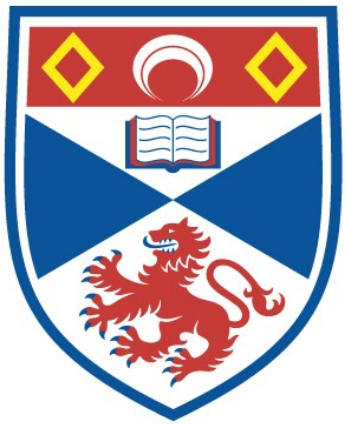

2004

Loop Oscillations in the Corona

Lorna James

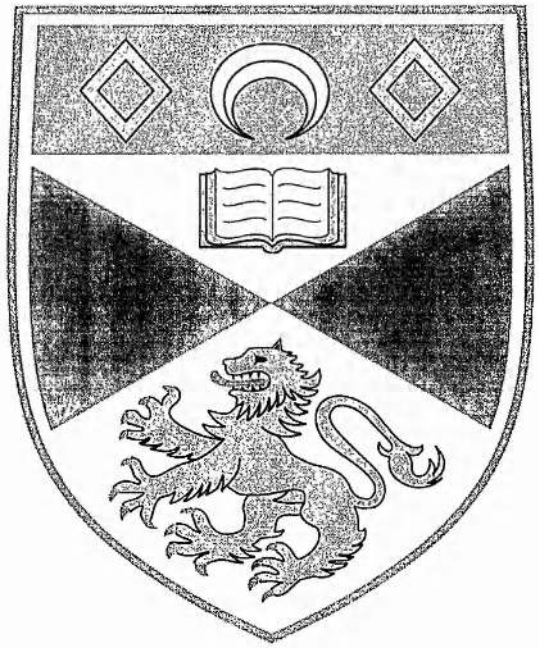

Thesis submitted for the degree of Master of Philosophy
of the University of St Andrews

9th February 2004

ProQuest LLC.
789 East Eisenhower Parkway
P.O. Box 1346
Ann Arbor, MI 48106 – 1346

Abstract

Magnetic loops in the Sun's corona have been discovered to oscillate in a variety of modes. The oscillations are observed to exhibit strong damping. A number of theories have been put forward to explain the damping, including resonant absorption and phase mixing. Here we consider the modelling of loop oscillations, paying particular attention to two effects: gravity, and the addition of a chromospheric layer below the corona.

We develop an acoustic model of coronal loop oscillations and consider two ways of describing the effects of the gravitational stratification and the chromospheric layers, considering either two media separated by a discontinuous interface or a single medium with a sound speed that varies along the loop.

A dispersion relation for the two-layer isothermal atmosphere case is obtained and investigated numerically using a bisection code. On comparison with roots obtained for a single isothermal atmosphere, it was found that the effect of chromospheric footpoints on the period of a mode is slight.

However, the effect of gravity was found to be more notable, rising up to a twenty percent change in period when considering the longer observed loops. This result is of especial interest since gravity is often ignored by authors discussing loop oscillations.

The case of a linear sound speed has been investigated analytically, obtaining a dispersion relation in terms of Bessel functions. Our results show that the Bessel equation is a possible solution for describing the wave modes.

Declaration

1. I, Lorna James, hereby certify that this thesis, which is approximately 16,000 words in length, has been written by me, that it is a record of work carried out by me and that it has not been submitted in any previous application for a higher degree.

   date ..... signature of candidate 21/04/04

2. I was admitted as a research student in October 2001 and as a candidate for the degree of MPhil in July 2003; the higher study for which this is a record was carried out in the University of St Andrews between 2001 and 2004.

   date ..... signature of candidate 21/04/04

3. I hereby certify that the candidate has fulfilled the conditions of the Resolution and Regulations appropriate to the degree of MPhil in the University of St Andrews and that the candidate is qualified to submit the thesis in application for that degree.

   date 21 April 2004 signature of supervisor .....

4. In submitting this thesis to the University of St Andrews I understand that I am giving permission for it to be made available for use in accordance with the regulations of the University Library for the time being in force, subject to any copyright vested in the work not being affected thereby. I also understand that the title and abstract will be published and that a copy of the work may be made and supplied to any *bona fide* library or research worker.

   date ..... signature of candidate 21/04/04

Acknowledgements

Many thanks to my supervisor, Prof. Bernard Roberts, for helping me to finish this thesis and submit my Masters.

Thanks to all the friends in St Andrews and beyond who have always been there for me.

I gratefully acknowledge the love and support of my special honey, Francois-Xavier.

Finally a special thankyou must go to my family for the many supportive phone conversations throughout my postgraduate and undergraduate life.

I am also grateful to PPARC for financial support.

Contents

1 Observations of loop oscillations **5**

1.1 The Sun 5
1.2 How we observe 7
1.3 Before TRACE 8
1.4 After TRACE 9
1.5 Damping 12
1.6 SUMER and slow waves 14

2 MHD waves **16**

2.1 MHD equations 16
2.2 Sound waves 17
2.3 Magnetic waves 19
2.4 Waves in a structured medium 23
2.5 Waves in a uniform medium 24
2.6 Waves at a magnetic interface 25
2.7 Waves in a magnetic slab 26
2.8 Waves in a magnetic flux tube 28
2.9 Gravity 30

3 Coronal loop oscillation model **35**

3.1 Coronal Loop model 35
3.2 Case 1 - Isothermal atmosphere 37
3.2.1 Dispersion relation 37
3.2.2 An isolated medium 39
3.2.3 Shallow chromospheric layer 40
3.2.4 Dimensionless dispersion relation 43
3.3 Case 2 - Continuous sound speed 46
3.3.1 Confirming the Bessel result 48
3.3.2 Dispersion relation 49

4 Results **52**
4.1 Effect of chromospheric layer 52
4.1.1 Checking numerical method 52
4.1.2 Numerical results 54
4.2 Effect of gravity 56
4.3 Applying theory to SUMER data 60

5 Conclusion **65**
5.1 Thesis summary 65
5.2 The impact of a chromospheric layer 66
5.3 The impact of gravity 66
5.4 Possible future work 66

A Boundary Condition **67**

B Dimensionless Dispersion Relation **70**

C Solar Values **72**

D Zeros of Cross-Products of Bessel Functions **74**

Bibliography **77**

List of Figures

1.1 The layers of our Sun 5
1.2 The rise in temperature above the solar surface 6
1.3 Coronal loop observed by TRACE 7
1.4 Spectrum of wavelengths 7
1.5 Radio pulsations 8
1.6 Loop oscillations on 14 July 1998 10
1.7 Damping of coronal loop 11
1.8 Histogram comparing TRACE and SUMER loops 15

2.1 A travelling wave 18
2.2 Polar plots of magnetoacoustic waves 21
2.3 Surface and body waves 22
2.4 Sausage and kink modes 22
2.5 Equilibrium magnetic interface 25
2.6 Equilibrium magnetic slab 26
2.7 Dispersion plot for magnetic surface waves 28
2.8 Wave modes in a magnetic cylinder 29

3.1 Coronal loop model 35
3.2 Simplified coronal loop model 36
3.3 Isolated slab 39
3.4 Sketch of the dimensionless wave frequency for an isolated coronal structure 45
3.5 Sketch of the period for an isolated coronal structure 45

4.1 Dispersion plot for small h 53
4.2 Dispersion diagram for small h 54
4.3 Dispersion diagram for large h 55
4.4 Impact of loop length on $\Delta\tau_{gravity}$ 60
4.5 The evolution of slow standing waves observed by SUMER . . . 64

List of Tables

1.1 Properties of TRACE loops 12
1.2 Properties of SUMER loops 15

3.1 Bessel asymptotic solutions 51

4.1 Comparison of wave frequency obtained numerically and analytically 53
4.2 Effect of chromosphere on period 56
4.3 Effect of gravity on period 59
4.4 SUMER waves compared to slow mode 61
4.5 SUMER waves compared to kink mode 62

Chapter 1

Observations of loop oscillations

1.1 The Sun

Our Sun is a star like all the others in the night sky. One property that makes the Sun unique is its distance from us; it is one Astronomical Unit away, approximately 1.5×10^{11} m (Priest 1982). The next closest star is Proxima Centauri at a distance of 4.29 light years, which is 271000 times farther away from us than the Sun. The Sun therefore gives us a unique opportunity to study in depth the physics of a star.

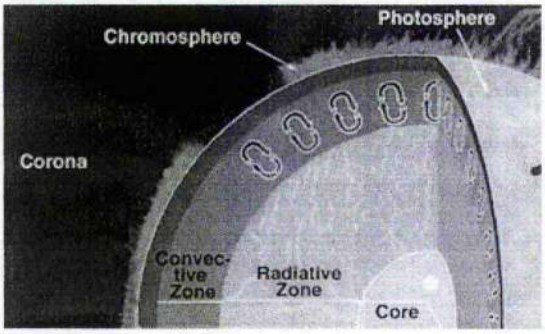

Figure 1.1: The layers of the Sun. [1]

The Sun can be thought of as having two parts, an interior and an atmosphere, the structure of which is shown in Figure 1.1. The inner Sun consists of the *core*, *radiative zone* and *convection zone* (see, for example, Ridpath 1997). The core is the centre of the Sun; here most of the Sun's energy is created by the fusion of hydrogen into helium. The radiative zone is so called because energy is transmitted through this region through radiative diffusion. Finally, in the

convection zone, energy is transmitted through overturning convective motions of the medium. These convective motions are observed at the solar surface as supergranules and granules.

The outer Sun consists of the *photosphere*, *chromosphere* and *corona*. The photosphere is thought of as the surface of the Sun as this is seen in normal light. Above the photosphere is the chromosphere. The corona is basically everything above the chromosphere spreading far out into space.

The corona is a very interesting medium with many puzzles still unanswered. A major puzzle is that of its temperature. The Sun's temperature gradually decreases from the core to the photosphere, dropping from 10^7 K to 6000 K. But in the thin transition region between the chromosphere and the corona the temperature rises abruptly to 2×10^6 K (see Figure 1.2).

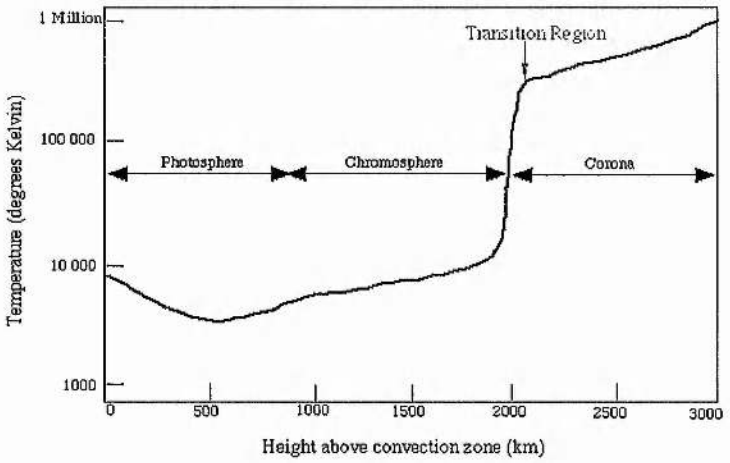

Figure 1.2: The rise in temperature above the solar surface. [2]

Dominated by its magnetic field, the corona is a very active part of the Sun. There are huge filaments or prominences, ribbons of cool dense gas that 'float' above the photosphere, held up by the magnetic field. There are coronal holes, where the magnetic field lines are open and stretch out into space. Coronal loops are large arch-shaped structures outlining the magnetic field. They appear to emerge from the photosphere below, possibly originating at a sunspot or regions of strong magnetic flux concentration and returning to the surface at another sunspot or regions of strong magnetic field (see Figure 1.3). The magnetic field and the plasma it entrains can become unstable, resulting in solar 'explosions' such as flares and coronal mass ejections (CMEs). These events release huge amounts of hot (10^6 K) plasma into space and propel vast quantities of high-speed particles ahead of them.

Figure 1.3: A coronal loop photographed by TRACE on 12 September 2000. [3]

1.2 How we observe

The corona is hard to observe from the Earth since the light from the photosphere dominates. It can be viewed during eclipses when that light is blocked out by the Moon, and scientists have learnt to make their own artificial eclipses. Telescopes were modified to have a disk in the middle which would block out the main part of the Sun. Such instruments are called coronagraphs and were first developed in 1930 (Lang 2001). It is also possible to analyse radio signals from the Sun. However, the corona is better observed in shorter wavelengths such as x-ray and extreme ultraviolet (see Figure 1.4).

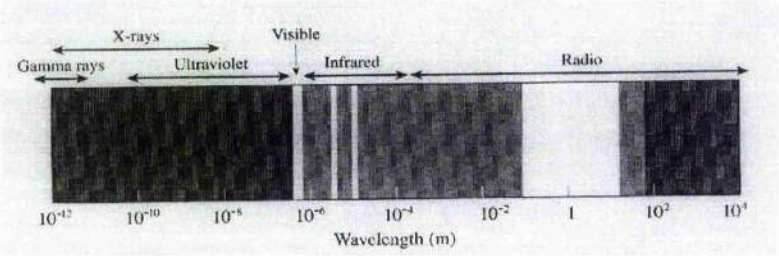

Figure 1.4: The spectrum of wavelengths. (Lang 2001)

The study of the Sun has changed dramatically since the advent of telescopes in space. *Yohkoh*, a Japanese satellite launched in 1991, has given an abundance of data (Ogawara *et al.* 1991), until it stopped transmitting on 14 December 2001. Its primary mission was to study solar flares at x-ray and gamma-ray wavelengths. The *SOlar and Heliospheric Observatory* (SOHO) was launched in December 1995 and started sending back data in February 1996 (Domingo *et al.* 1995). It was designed to help with answers to four key questions (Fleck *et al.* 1995): what is the nature of the solar interior and dynamo? How is the corona heated? What is the origin of CMEs? How is the solar wind

accelerated? SOHO has been successful in producing data for helioseismology, the study of the Sun's interior by observing the oscillations of its surface. The major instruments giving data for helioseismology are VIRGO, GOLF and MDI. VIRGO had the aim to determine the characteristics of long-wavelength global sound waves from irradiance variations (Fröhlich 1995). GOLF had the aim to study the internal structure of the Sun by measuring the spectrum of global oscillations in low frequency ranges (Gabriel *et al.* 1995). MDI provides scientists with magnetograms of the photosphere but it also detects modes of oscillation of the Sun and that data has been used to produce amazing spectrums of global oscillations (Scherrer *et al.* 1995). Another important instrument on SOHO is SUMER (Solar Ultraviolet Measurements of Emitted Radiation) (Wilhelm *et al.* 1995), a spectrometer (see section 1.6).

The spacecraft that has had the most impact on the study of oscillations of coronal loops is *Transition Region And Coronal Explorer* (TRACE). TRACE was launched in April 1998 and, with the help of filters to view different wavelengths, its aim was to study the connection between fine-scale magnetic fields and the associated plasma structures (Handy *et al.* 1998). TRACE has high cadences, with a time-cadence of 10 seconds and a spatial resolution of 0.5 arc-seconds. This is much greater than SOHO which has a cadence of 30 seconds and a resolution of 2.5 arc-seconds.

1.3 Before TRACE

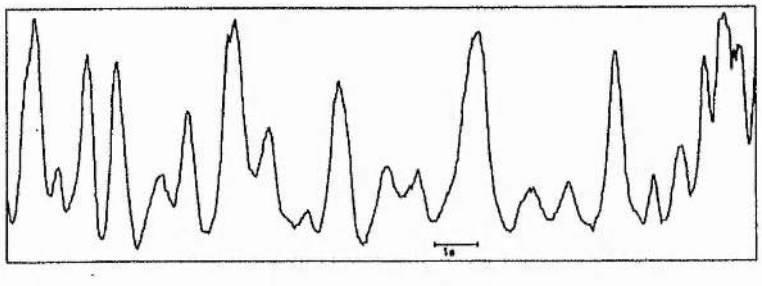

Figure 1.5: Microphotometric tracing of radio pulsations observed on February 25, 1969, 09:55 UT, in the frequency range of $\nu = 160 - 320$ MHz at the Utrecht radio observatory. Note that besides the fundamental mode of $P_1 \approx 3$ s, there are also subharmonic pulse structures with periods of $P_2 \approx 1$ s visible. (Rosenberg 1970)

In the early 70's, there were a number of papers analysing radio data (Rosenberg 1970; McLean and Sheridan 1973; see reviews by Aschwanden 1987, 2003). Rosenberg is often quoted for he observed standing waves with a period

$P = 0.5 - 5.0$ seconds (see Figure 1.5) and was the first to put a name to them, calling them 'radio pulsations'. It was not until later when more theoretical work was done (Roberts 1981a,b and Edwin and Roberts 1983) that a possible definition of oscillations observed by radio waves was suggested. Roberts, Edwin and Benz (1984) applied the theory of fast sausage MHD waves for a coronal plasma and used this to find the period,

$$P_{\text{fast sausage}} = 4\pi^{5/2} a \left(\frac{\rho_0 + \rho_e}{B_0^2 + B_e^2} \right)^{1/2} \approx \frac{2\pi a}{c_k}, \tag{1.1}$$

where a is the loop radius, c_k is the mean Alfvén speed and ρ_0, ρ_e and B_0, B_e are the density and magnetic field strength interior and exterior to the loop. Simply taking $a = 0.2h$, where h is the loop height, and $c_k = 1000 - 2000$ kms^{-1}, typical values for the corona, equation (1.1) gives

$$P = 0.1 - 5.0 \text{ seconds.}$$

This matched the range of periods observed by Rosenberg, so that a fast sausage mode seems to explain the observed periods.

1.4 After TRACE

TRACE, with its high spatial resolution, has produced amazing images of coronal loops (see Figure 1.3). Movies are produced showing actual spatial oscillations of loops. The first papers detailing oscillating loops, and many other phenomena, were by Schrijver *et al.* (1999) and Aschwanden *et al.* (1999). They reported on oscillations in spatial displacements observed following a flare at 12:55 UT on July 14, 1998 (see Figure 1.6). They studied nine loops, including groups of loops. Many general properties of oscillating loops suggested by this initial study have been confirmed by further investigation:

- EUV loops - the oscillations are observed in EUV light, at a temperature of 2×10^6K.
- Period length - The mean period for the loops in this study was $P = 280$ seconds, or around 5 minutes.
- Excitation - Aschwanden *et al.* observed a group of five loops oscillating almost in phase. This near simultaneous movement suggested to the authors that the excitation for the movement in the five individual loops was almost simultaneous. The close proximity of the loops to the flare,

and the timing, suggested a link between the onset of the oscillations and the flare, suggesting a possible driver for the oscillations.

- Wave type - standing fast kink mode.

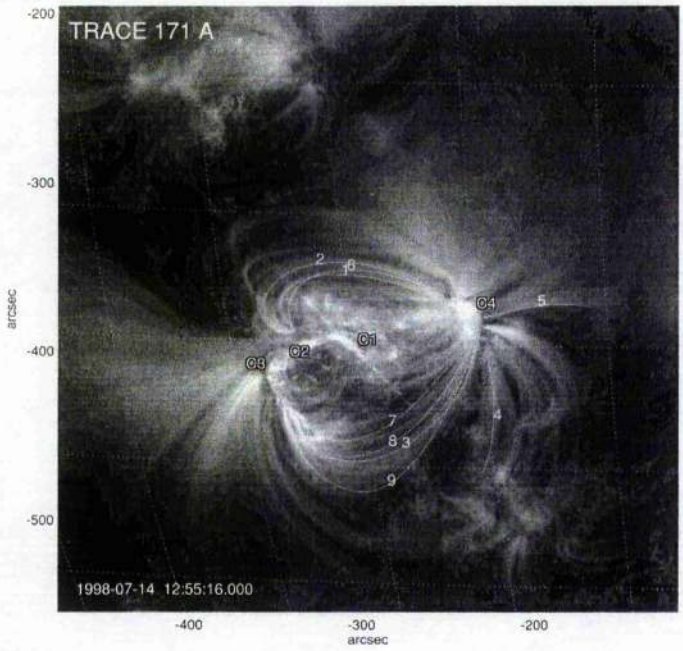

Figure 1.6: TRACE 171 image recorded at flare initiation, 1998 July 14, 12:55:16 UT, is shown with a logarithmic grey scale. The most prominent flare emission starts at location C_1 and progresses toward position C_3, straddling along the neutral line $C_1 - C_3$. The diagonal pattern across the brightness maximum at C_1 is a diffraction effect of the telescope. The analyzed loops are outlined by thin lines. Loop 4 and loops 6-9 show pronounced oscillations. (Aschwanden *et al.* 1999)

The last item, the wave mode, was found by Aschwanden *et al.* (1999) on consideration of all of the theoretically predicted modes of oscillation as given in Edwin and Roberts (1983). For the fast kink mode, the period is given by Edwin and Roberts to be

$$P_{fastkink} = \frac{2L}{jc_k} = 4\pi^{1/2}\frac{L}{j}\left(\frac{\rho_0 + \rho_e}{B_0^2 + B_e^2}\right)^{1/2}, \tag{1.2}$$

where j is wave mode, c_k is the phase speed, L is the loop length, $\rho_{0,e}$ is the ion mass density and $B_{0,e}$ is the magnetic field strength. On assuming $\rho_0 \ll \rho_e$ and $B_0 \approx B_e$, taking the first wave mode $j = 1$ and using typical parameters

of EUV loops, Aschwanden *et al.* found a mean period of $P_{fastkink} = 123$secs and a range of $P = 0.57.8$ minutes. From this conclusion, and on rejecting the possibilities of the fast sausage and slow modes, Aschwanden *et al.* concluded that the waves were fast kind modes. (See section 2.3 for a description of wave modes).

Independently, Nakariakov *et al.* (1999), also reported on the flare-oscillation event. They analysed a sequence of 88 images of active region AR8270, beginning at 12:11 UT. The major result from this study was the discovery of damping, shown in Figure 1.7. The damping time is found by fitting an exponential, e^{-t/τ_d}, to the oscillation curve which gives the decay time τ_d. The oscillating loop was measured to have a period $P = 256$ seconds and a damping time $\tau_d = 870$ seconds, corresponding to about 3 oscillation periods. This damping time, of 3 periods, is considered fast in solar terms and is a very interesting result.

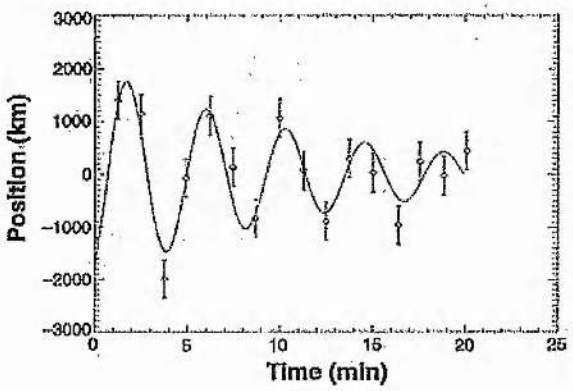

Figure 1.7: The temporal evolution of the loop displacement calculated as an average coordinate of the loop position for four neighbouring perpendicular cuts through the loop apex (diamonds), with error bars ($\pm$ 0.5 pixel). The oscillation started at 13:13:51 UT on 14 July, 1998. The solid curve is the best fit function to the oscillating displacements. (Nakariakov *et al.* 1999)

This was the first example of an oscillation of a coronal loop with strong damping. The scale of the damping has been confirmed by a study of 26 loops where the average was found to be $\tau_d/P = 4.0 \pm 1.8$ periods (Aschwanden *et al.* 2002). This study consisted of two papers. Analysing data from TRACE in the 171 and 195 wavelength bands, the authors looked at 17 flare and filament destabilisation events and found 26 individual oscillating loops. Schrijver *et al.* (2002) completed an extensive overview and analysis of the data, whilst Aschwanden *et al.* (2002) looked more at the physical parameters obtained

and gave a detailed discussion of these. The link between the flares and the oscillating loops seems to confirm the reason for excitation of the loops suggested by Aschwanden *et al.* (1999). However, the data is slightly biased as part of their data came from a survey of flares. Table 1.1 shows the periods and damping times found. The periods are nestled around the five minute band, so in general are longer than those observed by radio signals (where the periods are a few seconds). They found a variety of loop half-lengths, ranging from $36 - 291$Mm, although the largest loop appears to be spurious for the period of oscillations corresponding to this loop is over six times larger than the average period when this loop is neglected. Accordingly, we take the range of loop half-lengths to be 36-203 Mm, giving loops of length 72-406 Mm.

Parameter	Average	Range
Oscillation Period P	5.4 ± 2.3 min	2.3 - 10.8 min
Decay time τ_d	9.7 ± 6.4 min	3.2 - 20.8 min
Number of periods	4.0 ± 1.8	1.3 - 8.7

Table 1.1: Properties of Coronal loop oscillations. (After Aschwanden *et al.* 2002)

1.5 Damping

The reason for the strong damping is unknown although several theories have been put forward. These have been explored in some detail and a good review of possible processes involved in the damping is given in Roberts (2000).

Non-ideal effects, such as viscous and ohmic damping, optically thin radiation and thermal conduction can dampen waves. However, studies of both unbounded uniform medium (e.g. Ibañez and Escalona 1993) and a slab geometry (e.g. Laing and Edwin 1994) found the damping time to be at least 20 times the period, rising up to several hundred times. Thus, these effects are too small.

Wave leakage at the footpoints (De Pontieu *et al.* 2001) is too weak a damping force for standard chromospheric scale heights of the order $\Lambda = 500$km (Ofman 2002). However it could be an explanation if one takes a slightly larger scale height, say a factor of 2 bigger (Aschwanden *et al.* 2002).

Phase mixing (Heyvaerts and Priest 1983) and resonant absorption (Ionson 1978, Ruderman and Roberts 2002) are both promising ideas. Phase mixing considers the different propagation speeds that exist on different field lines, so that oscillations on neighbouring field lines become out of phase; this allows

cross-field gradients to build up, enhancing damping by viscosity or diffusivity. Resonant absorption is the process by which the global kink mode oscillation of a tube couples with Alfvénic oscillations. This means there is a transfer of energy from the global mode to small-scale oscillations resulting in a decay of the global mode. Resonant absorption has recently been reviewed by Erdélyi (2001).

Both phase mixing and resonant absorption are discussed in a recent review by Roberts (2000) and shown to be possible. Roberts looked at the process of phase mixing of an Alfvén wave. He considered an Alfvén wave in an inhomogeneous plasma with Alfvén speed $c_A(x)$, structured in x. This wave will propagate with transverse motions $v(x,z,t)\hat{y}$:

$$v = u(t)\ \sin k_z t \cos k_z c_A(x) t, \tag{1.3}$$

where k_z is the wave number and

$$u(t) = u_0 \exp\ -\frac{1}{2} k_z^2 \nu (t + \frac{1}{3}(c_A')^2 t^3), \tag{1.4}$$

where ν is the coefficient of kinematic viscosity.

Considering a uniform medium, so that $c_A' = 0$, a decay time τ_d is produced,

$$\tau_d = \frac{2}{\nu k_z^2}. \tag{1.5}$$

This produces a long decay time for a standing wave where $k_z = N\pi/L$, where N is the wave mode and L is the loop length. However in a magnetically structured plasma the later term in $u(t)$ dominates giving a decay time of

$$\tau_d = \left[\frac{6}{\nu k_z^2 (c_A')^2}\right]^{1/3}. \tag{1.6}$$

On the assumption of a spatially varying Alfvén speed, on a scale of order $l = L/10$, and taking a loop length of $L = 10^5$km and an Alfvén speed of $c_A = 10^3$km s^{-1}, a decay time $\tau_d = 530$s is obtained. This value is comparable with observed values and suggests that phase mixing or resonant absorption could be a viable reason for the strong damping of the oscillations.

Ofman and Aschwanden (2002) have considered phase mixing and resonant absorption further and argue that the observational data supports phase mixing more that resonant absorption. However, Ofman and Aschwanden (2002) make the assumption that the scale of inhomogeneity (that feeds the

phase mixing) is directly proportional to the length of the loop. There seems little reason to accept this assumption of proportionality, unless more compelling observational support is forthcoming. The theoretically predicted damping rate in resonant absorption (see Ruderman and Roberts 2002) is able to match the observational data for a reasonable range of the inhomogeneity scale l. For a tube of radius a, Ruderman and Roberts (2002) find that $l = 0.23a$, which matches the Nakariakov *et al.* event. A more extensive study by Goossens *et al.* (2002) supports this conclusion, producing a range of $l = 0.15a$ to $l = 0.5a$. See also the discussion in Roberts (2002). A very recent analysis by Aschwanden *et al.* (2003) offers further support for the resonant absorption idea but also points out that phase mixing remains a possibility.

1.6 SUMER and slow waves

Recent studies by Wang *et al.* al (2002c; 2002a,b), a group from the Max-Planck Institute in Germany, have considered Doppler shift oscillations using data from the SUMER spectrometer on SOHO. They found evidence of oscillations in hot active region loops which are markedly different from those observed by TRACE. Indeed, there is no sign of these oscillations in the TRACE lines of 2×10^6K; the oscillations are observed only in hot plasma greater than 6×10^6K.

- The oscillations coincide with loops seen in hot soft X-ray, not EUV, loops.
- Period - the SUMER oscillations have distinctly longer periods ($P =$ 17min) than the TRACE transverse oscillations, although they have a similar decay rate.
- The excitation of the oscillations is unclear as, unlike TRACE data, few events are associated with flares.
- Wave type - slow mode.

The definition of the waves as a slow mode was confirmed by Ofman and Wang (2002). They used a 1-D MHD code to model the hot loops and concluded that the waves are slow mode magnetoacoustic standing waves.

Very recently, Wang *et al.* (2003) surveyed a greater number of Doppler shift oscillations found by SUMER. They report on 54 such incidents in 27 events. To provide easy comparison with the TRACE loops, Table 1.2 gives the same parameters for the SUMER loops as Table 1.1 on the TRACE loops. Figure 1.8 provides histograms directly comparing four parameters. Wang *et*

Parameter	Average	Range
Oscillation Period P	17.6 $\pm$ 5.4 min	7.1 - 31.1 min
Decay time τ_d	14.6 $\pm$ 7.0 min	5.7 - 36.8 min
Number of periods	2.3 $\pm$ 0.7	1.5 - 5

Table 1.2: Properties of hot soft X-ray loop oscillations. (Wang *et al.* 2003)

al. (2003) conclude that the excitation of these oscillations may be pressure disturbances associated with the injection of hot plasma at the oscillating loop's footpoints.

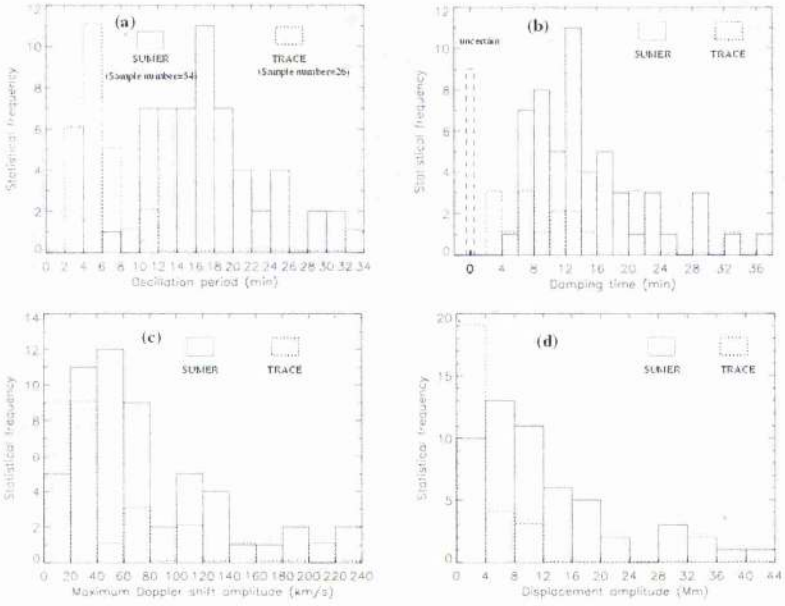

Figure 1.8: Distribution of the physical parameters of the 54 SUMER Doppler-shift oscillations (solid histograms), and distribution of the parameters of the 26 TRACE loop oscillations (dotted histograms) obtained by Aschwanden *et al.* (2002). **a**) Oscillation periods. **b**) Damping time. The number of TRACE loop oscillations whose damping time could not be evaluated is represented with a dashed strip. **c**) Measured maximum Doppler velocity amplitude for SUMER oscillations and the maximum transverse speed for TRACE oscillations. **d**) Derived displacement amplitude for SUMER oscillations, and the transverse motion amplitude for TRACE oscillations. Wang *et al.* (2003)

Chapter 2

MHD waves

Before a discussion on magnetohydrodynamic (MHD) waves in the solar atmosphere, it is necessary to consider some of the basic wave forms, their properties and how they relate to each other.

2.1 MHD equations

The solar atmosphere is a stratified and strongly structured magnetic medium. We use the equations of MHD to describe the wave motions that may occur. Taking velocity $\mathbf{v}$, magnetic field $\mathbf{B}$, pressure p, density ρ, gravity g, magnetic permeability μ and adiabatic index γ, we have:

- Equation of continuity

$$\frac{\partial \rho}{\partial t} + \mathrm{div}(\rho \mathbf{v}) = 0. \tag{2.1}$$

- Equation of motion

$$\rho \left(\frac{\partial \mathbf{v}}{\partial t} + (\mathbf{v} \cdot \nabla \mathbf{v}) \right) = -\nabla p + \frac{1}{\mu} (\nabla \times \mathbf{B}) \times \mathbf{B} + \rho \mathbf{g}. \tag{2.2}$$

- Induction equation

$$\frac{\partial \mathbf{B}}{\partial t} = \mathrm{curl}\,(\mathbf{v} \times \mathbf{B}), \tag{2.3}$$

  for an electrically ideal fluid.

- The solenoidal constraint from Maxwell's equations,

$$\nabla . \mathbf{B} = 0. \tag{2.4}$$

- Energy equation

$$\frac{\partial p}{\partial t} + \mathbf{v} \cdot \nabla p = \frac{\gamma p}{\rho} \left(\frac{\partial \rho}{\partial t} + \mathbf{v} \cdot \nabla \rho \right), \tag{2.5}$$

for an adiabatic medium.

- Perfect Gas Law

$$p = \frac{k_B}{\hat{m}} \rho T, \tag{2.6}$$

where k_B is the Boltzmann constant, $\hat{m}$ is the mean particle mass and T is the temperature.

2.2 Sound waves

In the absence of a magnetic field ($\mathbf{B} = 0$) and gravity ($g = 0$) we obtain the hydrodynamic equations with which we can investigate sound waves. Consider a compressible fluid at rest with undisturbed uniform pressure p_0 and density ρ_0. Suppose that as a result of a small disturbance the pressure and density are changed so that

$$p = p_0 + p_1, \quad \rho = \rho_0 + \rho_1,$$

where $p_1 \ll p_0$ and $\rho_1 \ll \rho_0$.

Linearising the equation of continuity (2.1) and the equation of motion (2.2) respectively, by neglecting squares of small quantities, we obtain

$$\frac{\partial \rho_1}{\partial t} + \rho_0 \text{div } \mathbf{v} = 0, \tag{2.7}$$

$$\rho_0 \frac{\partial \mathbf{v}}{\partial t} = -\nabla p_1. \tag{2.8}$$

Linearising the energy equation (2.5) and the perfect gas law (2.6) gives

$$\frac{\partial p_1}{\partial t} + \mathbf{v} \cdot \nabla p_0 = \frac{\gamma p_0}{\rho_0} \left(\frac{\partial \rho_1}{\partial t} + \mathbf{v} \cdot \nabla \rho_0 \right), \tag{2.9}$$

$$p_1 = \frac{k_B}{\hat{m}} \left(\rho_1 T_0 + \rho_0 T_1 \right), \tag{2.10}$$

with the equilibrium state

$$p_0 = \frac{k_B}{\hat{m}} \rho_0 T_0. \tag{2.11}$$

We introduce the sound speed c_s,

$$c_s = \left(\frac{\gamma p_0}{\rho_0}\right)^{1/2}. \tag{2.12}$$

Eliminating the pressure terms p_1 and p_0 from equation (2.8) using equations (2.9) and (2.11) and using the vector identity

$$\text{curl curl } \mathbf{v} = \text{grad div } \mathbf{v} - \nabla^2 \mathbf{v},$$

shows that $\mathbf{v}$ satisfies the 3-D wave equation,

$$\frac{\partial^2 \mathbf{v}}{\partial t^2} = c_s^2 \nabla^2 \mathbf{v}. \tag{2.13}$$

Thus, the solution of the hydrodynamic equations is a *sound* wave with speed c_s.

Without loss of generality, consider the x-component of velocity v_x. The general solution of (2.13) for v_x is

$$v_x = f(x - c_s t) + g(x + c_s t), \tag{2.14}$$

where $f(x)$ and $g(x)$ are arbitrary functions.

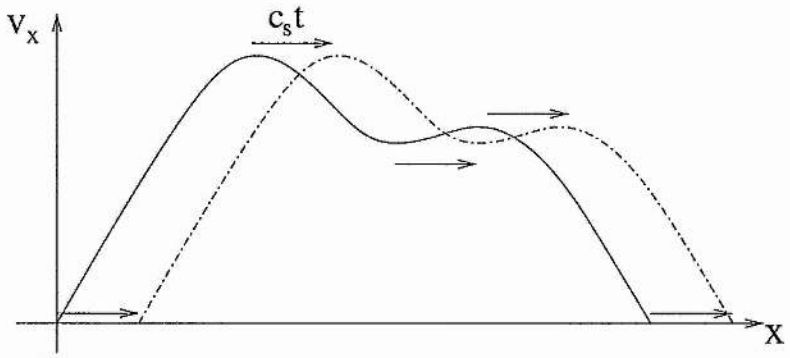

Figure 2.1: A wave of arbitrary shape travelling at speed c_s in the x-direction.

Consider $v_x = f(x - ct)$. In any plane x =constant, the velocity changes in time. However there exist co-ordinates x and t such that $x - c_s t$=constant, x =constant+$c_s t$ when v_x will have the same profile. This is illustrated in Figure 2.1. A wave such as this which propagates at a certain speed is called a *travelling* wave. The opposite of a travelling wave is a *standing* wave, where the wave oscillates but does not propagate. A sound wave is also a *longitudinal* wave, for the wave travels in the same direction as the motion of the fluid

particles. A wave where the particles oscillate in a direction perpendicular to the direction of the wave is called a *transverse* wave.

2.3 Magnetic waves

The presence of a magnetic field changes the situation. In an infinitely conducting fluid, the fluid particles are 'tied' to the magnetic lines of force. So any attempt to initiate a sound wave will result in variations in the magnetic field. In 1942 Hannes Alfvén pointed out that, by analogy with the transverse vibrations of stretched strings, these variations will cause local compressions and rarefactions of the lines of force, ie the lines of force may oscillate (Alfvén 1942). This is the simplest type of MHD wave, the so-called *Alfvén* wave.

Mathematically we need to consider the linearised forms of the equation of motion (2.2) and the induction equation (2.3). Write $\mathbf{B} = \mathbf{B}_0 + \mathbf{b}$, where $\mathbf{B}_0 = (0, 0, B_0)$ is the uniform background magnetic field and $\mathbf{b}$ is the perturbation where $|\mathbf{b}|$ is small. Recall the vector identity,

$$(\mathbf{a} \cdot \nabla)\mathbf{a} = \nabla \left(\frac{1}{2}a^2\right) - \mathbf{a} \times \operatorname{curl} \mathbf{a},$$

or

$$(\mathbf{B} \cdot \nabla)\mathbf{B} = \nabla \left(\frac{1}{2}B^2\right) + \operatorname{curl} \mathbf{B} \times \mathbf{B},$$

where $B = |\mathbf{B}| = B_0^2 + b^2 + 2\mathbf{B} \cdot \mathbf{b}$. Using this vector identity, the equation of motion (2.2) with $g = 0$ reduces to

$$\rho_0 \frac{\partial \mathbf{v}}{\partial t} = -\nabla \left(p_0 + \frac{B^2}{2\mu}\right) + \frac{B_0}{\mu} \frac{\partial \mathbf{b}}{\partial z}. \tag{2.15}$$

We restrict attention here to motions that are incompressible, so that $\operatorname{div}\mathbf{v} = 0$. Then considering the divergence of this equation and recalling that $\operatorname{div} \mathbf{B} = 0$, we find that

$$\nabla^2 \left(p + \frac{B^2}{2\mu}\right) = 0. \tag{2.16}$$

From this result, and the theorem of uniqueness of solutions to Laplace's equation, we can take $p_0 + \frac{B^2}{2\mu}$ equal to a constant. Since $\nabla(\text{constant}) = 0$, the linearised equation of motion (2.15) reduces to

$$\rho_0 \frac{\partial \mathbf{v}}{\partial t} = \frac{B_0}{\mu} \frac{\partial \mathbf{b}}{\partial z}. \tag{2.17}$$

Linearising the induction equation (2.3) using the vector identity

$$\text{curl}(\mathbf{a} \times \mathbf{b}) = \mathbf{a}\text{div}\,\mathbf{b} - \mathbf{b}\text{div}\,\mathbf{a} + (\mathbf{b} \cdot \nabla)\mathbf{a} - (\mathbf{a} \cdot \nabla)\mathbf{b},$$

gives

$$\frac{\partial \mathbf{b}}{\partial t} = B_0 \frac{\partial \mathbf{v}}{\partial z}. \tag{2.18}$$

Simply differentiating one of the equations (2.17) and (2.18) with respect to z and the other with respect to t shows that both $\mathbf{b}$ and $\mathbf{v}$ satisfy the wave equation

$$\frac{\partial^2}{\partial t^2}(\mathbf{v}, \mathbf{b}) = c_A^2 \frac{\partial^2}{\partial z^2}(\mathbf{v}, \mathbf{b}), \tag{2.19}$$

where c_A is the *Alfvén* speed given by

$$c_A^2 = \frac{B_0^2}{\rho_0 \mu_0}. \tag{2.20}$$

There are also motions with div $\mathbf{v}$ non-zero; these are the magnetoacoustic modes, found by considering how all the linearised equations interact. Taking $p = p_0 + p_1$, $\rho = \rho_0 + \rho_1$, $\mathbf{B} = \mathbf{B}_0 + \mathbf{b}$, as before, the linearised MHD equations are:

$$\frac{\partial \rho_1}{\partial t} + (\mathbf{v} \cdot \nabla)\rho_0 + \rho_0(\nabla \cdot \mathbf{v}) = 0, \tag{2.21}$$

$$\rho_0 \frac{\partial \mathbf{v}}{\partial t} = -\nabla p_1 + \frac{1}{\mu}(\nabla \times \mathbf{b}) \times \mathbf{B}_0, \tag{2.22}$$

$$\frac{\partial \mathbf{b}}{\partial t} = \nabla \times (\mathbf{v} \times \mathbf{B}_0), \tag{2.23}$$

$$\frac{\partial p_1}{\partial t} + \mathbf{v} \cdot \nabla p_0 = c_s^2 \left(\frac{\partial \rho_1}{\partial t} + \mathbf{v} \cdot \nabla \rho_0 \right). \tag{2.24}$$

Differentiating (2.22) with respect to t and substituting for $\frac{\partial p_1}{\partial t}$ from (2.24) and for $\frac{\partial b}{\partial t}$ from (2.23) gives:

$$\rho_0 \frac{\partial^2 \mathbf{v}}{\partial t^2} = c_s^2 \nabla(\nabla \cdot \mathbf{v}) + \nabla \times (\nabla \times (\mathbf{v} \times \mathbf{B}_0)) \times \frac{\mathbf{B}_0}{\mu}. \tag{2.25}$$

We consider a Fourier component

$$\mathbf{v} \propto \exp i(\omega t + k_x x + k_y y + k_z z),$$

where $\mathbf{k} = (k_x, k_y, k_z)$ is the wavenumber vector of magnitude $|\mathbf{k}| = k = (k_x^2 + k_y^2 + k_z^2)^{1/2}$. Let the direction of propagation vector $\mathbf{k}$ be at an angle θ to the equilibrium magnetic field $\mathbf{B_0}$. Then equation (2.25) gives the dispersion relation

$$\omega^4 - (c_A^2 + c_s^2)\omega^2 k^2 + c_A^2 c_s^2 k^4 \cos^2\theta = 0, \tag{2.26}$$

where θ is the angle between $\mathbf{k}$ and $\mathbf{B_0}$; dispersion relation 2.26 has two real roots for ω^2 (four roots for ω). In general, including the Alfvén wave there are three distinct waves: the Alfvén wave is one, and the other two are *magnetoacoustic* waves which are called the *fast* and *slow* waves. The relative wave speeds of the solutions of equation (2.26) can be seen by polar plots of the phase speed ω/k, displayed in Figure 2.2 as a function of θ. The fast wave speed c_f

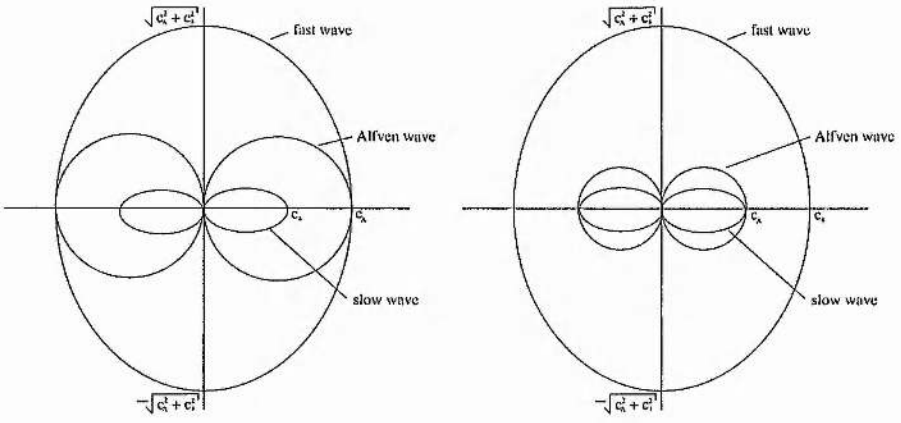

(a) $c_A > c_s$ (b) $c_A < c_s$

Figure 2.2: Polar plots of the three MHD wave speeds.

is both super-sonic and super-Alfvénic and is associated with the speed c_{fast} which can be written in terms of c_s and c_A through (Roberts 1991)

$$c_{fast}^2 = c_s^2 + c_A^2. \tag{2.27}$$

The slow wave speed is both sub-sonic and sub-Alfvénic and is associated with the speed c_{slow} (or c_T) which can be written in terms of c_s and c_A through (Roberts 1991)

$$\frac{1}{c_{slow}^2} = \frac{1}{c_s^2} + \frac{1}{c_A^2} \quad \text{or} \quad c_{slow}^2 = c_T^2 = \frac{c_s^2 c_A^2}{c_s^2 + c_A^2}. \tag{2.28}$$

This speed generally arises in the modelling of waves in a flux tube and so is commonly called the *tube* speed.

Another property of waves to consider is the shape of the waves. For waves propagating in non-uniform media, say in a flux-tube or across an interface, either *surface* or *body* waves can arise (see Figure 2.3). The surface wave is located predominant at boundaries, whilst body waves exist throughout.

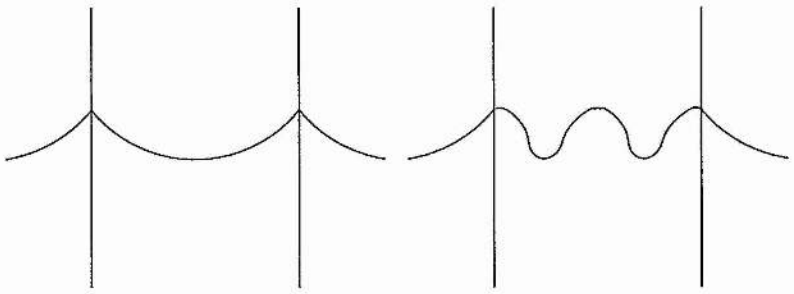

(a) Surface wave (b) Body wave

Figure 2.3: Waves profiles across a flux tube or slab (After Roberts 1981a,b; Edwin and Roberts 1983)

Also, for a magnetic slab or tube these modes may be geometrically classified as *sausage* or *kink* modes (see Figure 2.4).

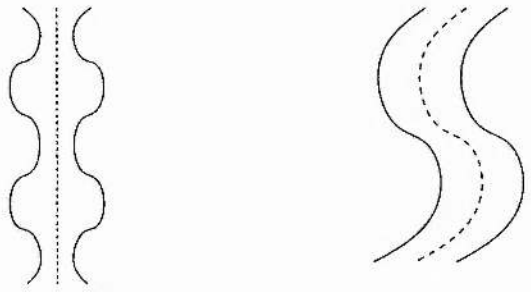

(a) Sausage mode (b) Kink mode

Figure 2.4: Modes of oscillation of a magnetic flux tube

The sausage mode is a symmetric pulsation of the tube and corresponds to the velocity component $\mathbf{v}_x$ (or $\mathbf{v}_r$) being an odd function of x (or r), giving a symmetric pulsation of the slab (or tube). The kink mode is an asymmetric distortion of the tube as a whole and corresponds to the transverse component of velocity of x (or r). There are also *standing* waves (oscillations) and *propagating*

(or *travelling*) waves in which the energy is transferred by means of vibrations, like waves on a string.

2.4 Waves in a structured medium

Consider a basic state in which there is a magnetic field of strength B_0 aligned with the z-axis in a Cartesian co-ordinate system. Let ρ_0, p_0 and B_0 all vary in a direction perpendicular to the applied magnetic field. With an equilibrium condition of pressure balance, we have a basic plasma state of the form

$$p_0 = p_0(x),\ \rho_0 = \rho_0(x),\ \frac{d}{dx}\left(p_0 + \frac{B_0^2}{2\mu}\right) = 0. \tag{2.29}$$

Suppose that as a result of a small disturbance the pressure, density and magnetic field are changed so that $p = p_0 + p_1$, $\rho = \rho_0 + \rho_1$, $\mathbf{B} = \mathbf{B}_0 + \mathbf{b}$, where $p_1 \ll p_0$, $\rho_1 \ll \rho_0$, $|\mathbf{B}_0| \ll |\mathbf{b}|$. Linearising the equations of continuity, motion, induction and energy equations (2.1)-(2.5), with $g = 0$, results in

$$\begin{aligned}
\frac{\partial \rho_1}{\partial t} + \operatorname{div}(\rho_0 \mathbf{v}) &= 0, \\
\rho_0 \frac{\partial \mathbf{v}}{\partial t} &= -\nabla\left(p_1 + \frac{1}{\mu}\mathbf{B}_0 \cdot \mathbf{b}\right) + \frac{1}{\mu}(\mathbf{B}_0 \cdot \nabla)\mathbf{b} + \frac{1}{\mu}(\mathbf{b} \cdot \nabla)\mathbf{B}_0, \\
\frac{\partial \mathbf{b}}{\partial t} &= \operatorname{curl}(\mathbf{v} \times \mathbf{B}_0), \qquad \nabla \cdot \mathbf{b} = 0, \\
\frac{\partial p_1}{\partial t} + \mathbf{v} \cdot \nabla p_0 &= c_s^2\left(\frac{\partial \rho_1}{\partial t} + \mathbf{v} \cdot \nabla \rho_0\right),
\end{aligned} \tag{2.30}$$

where $c_s = (\gamma p_0(x)/\rho_0(x))^{1/2}$ is the local sound speed (a function of x). Using the variables

$$\nabla = \operatorname{div} \mathbf{v},\ \Gamma = \frac{\partial v_z}{\partial x},\ p_T = p + \frac{1}{\mu}\mathbf{B}_0 \cdot \mathbf{b}, \tag{2.31}$$

the linearised equations (2.30) yield three partial differential equations (see, for example, Roberts 1981a)

$$\rho_0\left(\frac{\partial^2}{\partial t^2} - c_A^2\frac{\partial^2}{\partial z^2}\right)v_x = \frac{\partial}{\partial x}\left(\rho_0\left(c_s^2 + c_A^2\right)\Delta - \rho_0 c_A^2 \Gamma\right), \tag{2.32a}$$

$$\rho_0\left(\frac{\partial^2}{\partial t^2} - c_A^2\frac{\partial^2}{\partial z^2}\right)v_y = \frac{\partial}{\partial y}\left(\rho_0\left(c_s^2 + c_A^2\right)\Delta - \rho_0 c_A^2 \Gamma\right), \tag{2.32b}$$

$$\frac{\partial^2 v_z}{\partial t^2} = c_s^2\frac{\partial \Delta}{\partial z}. \tag{2.32c}$$

These three equations (2.32) can be reduced to a single ordinary differ-

ential equation by taking Fourier components. Writing

$$v_x = \hat{v}_x(x) \exp i(\omega t + k_y y + k_z z),$$

the governing differential equation is (Roberts 1981a)

$$\frac{d}{dx}\left(\frac{\rho_0(x)(k_z^2 c_A^2(x) - \omega^2)}{m^2(x) + k_y^2}\frac{d\hat{v}_x}{dx}\right) = \rho_0(x)(k_z^2 c_A^2(x) - \omega^2)\hat{v}_x, \tag{2.33}$$

where

$$m^2 = \frac{(k_z^2 c_s^2(x) - \omega^2)(k_z^2 c_A^2(x) - \omega^2)}{(c_s^2(x) + c_A^2(x))(k_z^2 c_T^2(x) - \omega^2)}; \tag{2.34}$$

the quantity m^2, introduced in the above, may be positive or negative.

Solutions of this equation are not straightforward. In particular, there exists continuous spectra of solutions connected with the singularities at $\omega^2 = k_z^2 c_A^2(x)$ and $\omega^2 = k_z^2 c_T^2(x)$. Two special cases most frequently analysed are the magnetic interface and the magnetic flux tube. However, the simplest case to consider first is when ρ_0, c_A and c_s are all constants, corresponding to a uniform unbounded atmosphere.

2.5 Waves in a uniform medium

For a uniform medium, equation (2.33) reduces to

$$(k_z^2 c_A^2 - \omega^2)\left(\frac{d^2\hat{v}_x}{dx^2} - (m^2 + k_y^2)v_x\right) = 0. \tag{2.35}$$

This equation yields the Alfvén wave, $\omega^2 = k^2 c_A^2$, with the form of $v_x(x)$ arbitrary (and determined by initial conditions). On taking a Fourier component $v_x \propto \exp(ik_x x)$, the differential operator in equation (2.35) yields the magnetoacoustic waves,

$$m^2 + k_x^2 + k_y^2 = 0; \tag{2.36}$$

that is

$$\omega^4 + k^2 k_z^2 c_s^2 c_A^2 - \omega^2 k^2 (c_s^2 + c_A^2) = 0,$$

where $k^2 = k_x^2 + k_y^2 + k_z^2$.

Equation (2.36) shows that $m^2 < 0$. Looking at equation (2.34) for m^2,

this implies ω^2/k_z^2 lies between c_T^2 and the smaller of c_s^2 and c_A^2, corresponding to a slow wave, or above the larger of c_s^2 and c_A^2, corresponding to the fast wave.

2.6 Waves at a magnetic interface

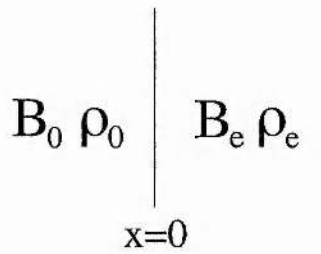

Figure 2.5: A magnetic interface x=0 separating a plasma with density ρ_0 and field strength B_0 in $x < 0$ from a plasma with density ρ_e and field strength B_e in $x > 0$.

A medium with an interface across which the physical properties change sharply can support surface waves. Consider an interface where the magnetic field changes discontinuously from a constant B_0 to a constant B_e, so that

$$B_0(x) = \begin{cases} B_0, & x < 0, \\ B_e, & x > 0, \end{cases} \tag{2.37}$$

as shown in Figure 2.5.

For a uniform medium, and ignoring Alfvén waves by setting $v_y = 0$ and $k_y = 0$, equation (2.33) reduces (in $x < 0$) to

$$\frac{d^2\hat{v}_x}{dx^2} - m^2\hat{v}_x = 0, \tag{2.38}$$

where

$$m^2 = m_0^2 = \frac{(k_z^2c_{s0}^2 - \omega^2)(k_z^2c_{A0}^2 - \omega^2)}{(c_{s0}^2 + c_{A0}^2)(k_z^2c_{T0}^2 - \omega^2)}; \tag{2.39}$$

here c_{s0} is the sound speed and c_{A0} is the Alfvén speed in $x < 0$. In the region $x > 0$, $m^2 = m_e^2$ and generally the '0' subscripts are replaced by 'e' subscripts. Thus the differential equation (2.38) has a simple exponential solution,

$$\hat{v}_x(x) = \begin{cases} \alpha_0 e^{m_0 x}, & x < 0, \\ \alpha_e e^{-m_e x}, & x > 0. \end{cases} \tag{2.40}$$

Assuming that $\hat{v}_x(x) \to 0$ as $|x| \to \infty$ requires that $m_0, m_e > 0$. A condition of continuous velocity at $x = 0$ is satisfied by taking $\alpha_0 = \alpha_e$.

A second boundary condition is that of continuous total pressure at the interface. To apply this, we need an equation relating $\hat{v}_x$ and $\hat{p}_T$, namely

$$\hat{p}_T = \frac{\rho_0(k_z^2 c_{A0}^2 - \omega^2)}{m_0^2} \frac{d\hat{v}_x}{dx}, \quad x < 0, \tag{2.41}$$

with a similar expression applying for $x > 0$ with 'e 'subscripts. Using (2.41) yields the dispersion relation (Roberts 1981a)

$$\rho_0(k_z^2 c_{A0}^2 - \omega^2)m_e + \rho_e(k_z^2 c_{Ae}^2 - \omega^2)m_0 = 0. \tag{2.42}$$

This is the dispersion relation governing magnetoacoustic surface waves on a single interface. Rewriting (2.42),

$$\frac{c_{A0}^2 - \omega^2/k_z^2}{c_{Ae}^2 - \omega^2/k_z^2} = -\frac{m_0\rho_e}{m_e\rho_0}, \tag{2.43}$$

implies the left-hand side of the fraction mush be negative, since $m_0, m_e > 0$. For this to be true ω/k_z must lie between the Alfvén speeds of the two media. It is found that in general there are two surface waves, the slow and fast waves (Roberts 1981a).

2.7 Waves in a magnetic slab

Flux tubes are an important consideration for the solar atmosphere. A first approximation to a flux tube is a magnetic slab, which is mathematically easier to discuss than the cylindrical geometry of a flux tube. The magnetic flux tube is discussed separately (see Section 2.8).

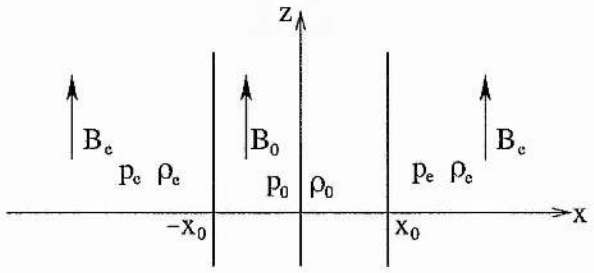

Figure 2.6: The equilibrium structured atmosphere of a magnetic slab.

Mathematically, the description of the equilibrium state is:

$$p_0(x), \rho_0(x), B_0(x) = \begin{cases} p_0, \rho_0, B_0, & |x| < x_0, \\ p_e, \rho_e, B_e, & |x| > x_0. \end{cases} \tag{2.44}$$

The magnetic slab is very similar to the magnetic interface, but with two boundaries at which the physical properties change sharply. Mathematically, the only difference is the equilibrium state, which is more bounded. Consequently the flow $\hat{v}_x$ is described by the solution of the differential equation (2.38) with $\hat{v}_x \to 0$ as $|x| \to \infty$:

$$\hat{v}_x(x) = \begin{cases} \alpha_e e^{m_e(x-x_0)}, & x < -x_0, \\ \alpha_0 \cosh\ m_0 x + \beta_0 \sinh\ m_0 x, & |x| < x_0, \\ \beta_e e^{-m_e(x-x_0)}, & x > x_0, \end{cases} \tag{2.45}$$

where $\alpha_e, \alpha_0, \beta_e, \beta_0$ are constants and $m_{0,e}$ are given as in Equation (2.39). It is necessary that $m_e > 0$ (to satisfy $\hat{v}_x \to 0$ as $|x| \to \infty$), but m_0^2 may be positive or negative (so m_0 may be positive or imaginary).

To consider odd solutions take $\alpha_0 = 0$, and for even solutions take $\beta_0 = 0$. Applying continuous boundary conditions at $x = \pm x_0$ for velocity and pressure, as in the case of the single interface, gives a series of relationships for the constants in equation (2.45). Ensuring a non-trivial solution determines the dispersion relation (Edwin and Roberts 1982),

$$\rho_e(k_z^2 c_{Ae}^2 - \omega^2) \begin{Bmatrix} \tanh \\ \coth \end{Bmatrix} m_0 x_0 + \rho_0(k_z^2 c_{A0}^2 - \omega^2) m_e = 0, \tag{2.46}$$

where 'tanh' corresponds to the odd solution and so is called the sausage mode, and 'coth' corresponds to the even solution and so is called the kink mode. As noted earlier, m_e is taken to be positive, whereas m_0^2 may be positive or negative.

For the special case of an incompressible fluid, m_0 and m_e tend to k_z, giving

$$\frac{\omega^2}{k_z^2} = \frac{\rho_0 c_{A0}^2 + \rho_e c_{Ae}^2 \begin{Bmatrix} \tanh \\ \coth \end{Bmatrix} k_z x_0}{\rho_0 + \rho_e \begin{Bmatrix} \tanh \\ \coth \end{Bmatrix} k_z x_0}. \tag{2.47}$$

Relating the magnetic slab to a flux tube, so that it resembles a coronal loop, consider a slender slab. Slender implies looking at the propagation of waves whose wavelength in much greater than the width of the slab, i.e. $k_z x_0 \ll 1$. So taking $\tanh k_z x_0 \approx k_z x_0$ and $\coth k_z x_0 \approx 1/k_z x_0$, equation (2.47) reduces to

$$\omega^2 \approx \begin{cases} k_z^2 c_{A0}^2 (1 + \rho_e/\rho_0 (c_{Ae}^2/c_{A0}^2 - 1) k_z x_0), & \text{for the sausage mode,} \\ k_z^2 c_{Ae}^2 (1 + \rho_0/\rho_e (c_{A0}^2/c_{Ae}^2 - 1) k_z x_0), & \text{for the kink mode.} \end{cases} \tag{2.48}$$

These results are displayed in a dispersion diagram (see Figure 2.7), which also shows the behaviour for general $k_z x_0$.

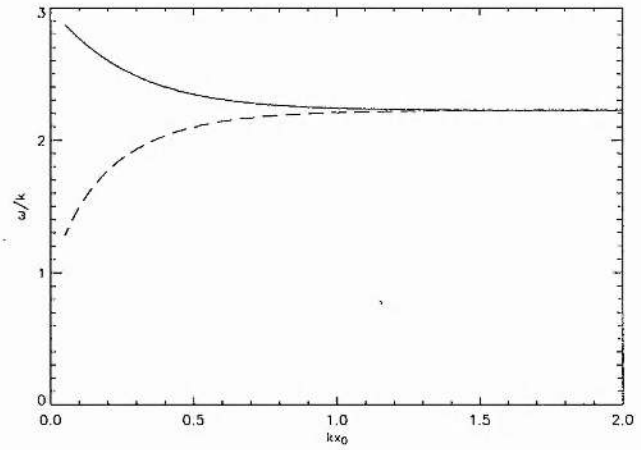

Figure 2.7: The phase speed ωk_z as of a function of $k_z x_0$ for magnetic surface waves in an incompressible medium with $c_{A0} < c_{Ae}$. A full curve represents the sausage mode and a dashed curve the kink mode. (Note: $k \equiv k_z$.)

For a more complete description of the solutions of Equation (2.46), see Edwin and Roberts (1982, 1983).

2.8 Waves in a magnetic flux tube

A better model of a flux tube can be obtained by using a cylindrical system instead of cartesian co-ordinates. The equilibrium setup is the same as for a magnetic slab except that the interface is $r = a$ instead of $x = \pm x_0$. Analogous equations to Equations (2.32) are found which can be reduced to an ordinary differential equation by taking Fourier components. Writing

$$\Delta = R(r) \exp i(\omega t + n\theta + kz), \tag{2.49}$$

the governing differential equation for $R(r)$ is

$$\frac{d^2R}{dr^2} + \frac{1}{r}\frac{dR}{dr} - \left(m_0^2 + \frac{n^2}{r^2}\right) R = 0. \tag{2.50}$$

This is a Bessel equation. Taking a bounded solution at $r = 0$ and no radial propagation of energy in $r > a$, there is a simple Bessel solution,

$$R(r) = \begin{cases} A_0 \begin{cases} I_n(m_0 r), & m_0^2 > 0 \\ J_n(n_0 r), & n_0^2 = -m_0^2 > 0 \end{cases} & r < a \\ A_1 \, K_n(m_e r), & r > a, \end{cases} \tag{2.51}$$

where A_0 and A_1 are constants and I_n, J_n and K_n are Bessel functions of order n (Abramowitz and Stegun 1964). As with the magnetic slab, taking continuous velocity and pressure at the interface $r = a$ yields a dispersion relation.

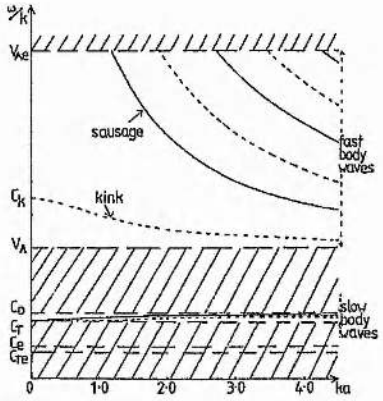

Figure 2.8: The phase-speeds ω/k_z of body modes under coronal conditions ($c_{Ae}, c_A > c_{se}, c_{s0}$), according to Edwin and Roberts (1983). (Note: $k \equiv k_z$, $v_{Ae} \equiv c_{Ae}$, $v_A \equiv c_A$.)

Considering $m_0^2 = -n_0^2 < 0$, the dispersion relation is (Edwin and Roberts 1983)

$$\rho_e(k^2 c_{Ae}^2 - \omega^2) n_0 \frac{J_n'(n_0 a)}{J_n(n_0) a} + \rho_0(k^2 c_{A0}^2 - \omega^2) m_e \frac{K_n'(m_e a)}{K_n(m_e a)} = 0. \tag{2.52}$$

Figure 2.8 illustrates the behaviour of waves under coronal conditions, i.e. when $c_{Ae}, c_{A0} > c_{se}, c_{s0}$. Edwin and Roberts discovered that in such circumstances there are no surface waves, just fast and slow body waves.

2.9 Gravity

The model we investigate looks at two new effects, one of which is the influence of gravity. It is a basic problem to consider the acoustic equations (i.e. the MHD equations with $\mathbf{B} = 0$) and including the stratification effect of uniform gravity $\mathbf{g} = (0, 0, g)$. The effect of gravity seriously complicates any discussion of magnetohydrodynamics. Here, we take a first step in this investigation by considering what happens to acoustic waves in the absence of a magnetic field. We may expect that in the presence of a magnetic field, slow waves will behave rather similarly to sound waves.

In the absence of a magnetic field, but with gravity present, the governing system of equations is now

$$\frac{\partial \rho}{\partial t} + \operatorname{div}(\rho \mathbf{v}) = 0, \tag{2.53}$$

$$\rho\left(\frac{\partial \mathbf{v}}{\partial t} + (\mathbf{v} \cdot \nabla \mathbf{v})\right) = -\nabla p + \rho \mathbf{g}, \tag{2.54}$$

$$\frac{\partial p}{\partial t} + \mathbf{v} \cdot \nabla p = c_s^2 \left(\frac{\partial \rho}{\partial t} + \mathbf{v} \cdot \nabla \rho\right), \tag{2.55}$$

$$p = \frac{k_B}{m} \rho T. \tag{2.56}$$

To examine the equilibrium state of this system, consider what happens when $\mathbf{v} = \mathbf{0}$ and $\frac{\partial}{\partial t} \equiv 0$. The momentum equation (2.54) reduces to

$$-\nabla p_0 + \rho_0 \, g \, \mathbf{e}_z = 0,$$

that is,

$$\frac{dp_0}{dz} = \rho_0 g. \tag{2.57}$$

The z-axis has been aligned with the direction of gravity, pointing downwards.

The perfect gas law (2.56) provides a relationship between p_0 and ρ_0,

$$p_0 = \frac{k_B}{m} \rho_0 T_0. \tag{2.58}$$

We consider T_0 to be a function of z only, i.e. $T_0 = T_0(z)$ for some arbitrary temperature distribution. Combining these two equilibrium equations by sub-

stituting $\rho_0(z) = \frac{p_0(z)m}{k_B T_0(z)}$ into equation (2.57) we obtain

$$\begin{aligned} \frac{dp_o}{dz} &= \frac{mg}{k_B T_0} p_0, \\ \frac{1}{p_0} dp_0 &= \frac{mg}{k_B T_0} dz. \end{aligned} \tag{2.59}$$

Thus

$$p_0 = p_0(0) = \exp\left(\int_0^z \frac{mg}{k_B T_0} dz \right). \tag{2.60}$$

Introducing Λ_0, the equilibrium pressure scale height, defined by

$$\Lambda_0(z) = \frac{k_B T_0(z)}{mg} = \frac{p_0}{\rho_0 g}, \tag{2.61}$$

gives

$$p_0(z) = p_0(0) \ \exp n(z), \qquad n(z) = \int_0^z \frac{dz}{\Lambda_0(z)}. \tag{2.62}$$

Equation (2.62) gives the distribution of equilibrium pressure $p_0(z)$ in terms of the pressure $p_0(0)$ at the arbitrary reference point $z = 0$ and the pressure scale height $\Lambda_0(z)$.

Linearising the system by taking

$$\rho = \rho_0(z) + \rho_1(x, z, t), \ p = p_0(z) + p_1(x, z, t),$$

where $\rho_1 \ll \rho_0$, $p_1 \ll p_0$, and taking

$$\mathbf{v} = (v_x, 0, v_z),$$

we produce the following set of linearised hydrodynamic equations:

$$\frac{\partial \rho_1}{\partial t} + \rho_0 \Delta + v_z \rho_0' = 0, \tag{2.63}$$

$$\rho_0 \frac{\partial v_x}{\partial t} = -\frac{\partial p_1}{\partial x}, \tag{2.64}$$

$$\rho_0 \frac{\partial v_z}{\partial t} = -\frac{\partial p_1}{\partial z} + g\rho_1, \tag{2.65}$$

$$\frac{\partial p_1}{\partial t} + g\rho_0 v_z = c_s^2 \left(\frac{\partial \rho_1}{\partial t} + v_z \rho' \right). \tag{2.66}$$

Here we have written $\Delta = \operatorname{div} \mathbf{v}$ and we have used the fact that ∇p_0 and $\rho_0 \, g \, \mathbf{e}_z$ cancel according to the equilibrium condition.

Differentiating equation (2.65) with respect to t gives

$$\rho_0 \frac{\partial^2 v_z}{\partial t^2} = -\frac{\partial^2 p_1}{\partial t\, \partial z} + g\frac{\partial \rho_1}{\partial t}.$$

We can substitute for $\frac{\partial \rho_1}{\partial t}$ from equation (2.63) to obtain

$$\rho_0 \frac{\partial^2 v_z}{\partial t^2} = -\frac{\partial^2 p_1}{\partial t\, \partial z} - g\rho_0 \Delta - g v_z \rho_0'. \tag{2.67}$$

We can then substitute $\frac{\partial p_1}{\partial t}$ in terms of ρ_0 and v_z only, by considering equation (2.66):

$$\begin{aligned}
\frac{\partial p_1}{\partial t} &= c_s^2 \left(\frac{\partial \rho_1}{\partial t} + v_z \rho_0' \right) - g\, \rho_0\, v_z \\
&= c_s^2 \left(-\rho_0 \nabla - v_z \rho_0' \right) + c_s^2 v_z \rho_0' - g\, \rho_0\, v_z \\
&= -c_s^2 \rho_0 \nabla - g\, \rho_0\, v_z.
\end{aligned} \tag{2.68}$$

Substituting this result into equation (2.67) reduces the equation to one containing only the variables ρ_0 and v_z and their derivatives:

$$\begin{aligned}
\rho_0 \frac{\partial^2 v_z}{\partial t^2} &= -\frac{\partial}{\partial z}\left[-c_s^2 \rho_0 \Delta - g\, \rho_0\, v_z \right] - g\rho_0 \Delta - g v_z \rho_0' \\
&= c_s^2 \rho_0 \frac{\partial \Delta}{\partial z} + \Delta \left[c_s^2 \rho_0' + \rho_0 (c_s^2)' \right] + g\rho_0 \frac{\partial v_z}{\partial z} + g v_z \rho_0' - g\rho_0 \Delta - g v_z \rho_0' \\
&= c_s^2 \rho_0 \frac{\partial \Delta}{\partial z} + \Delta \left[c_s^2 \rho_0' + \rho_0 \left(\gamma g - \frac{c_s^2 \rho_0'}{\rho_0} \right) \right] + g\rho_0 \frac{\partial v_z}{\partial z} - g\rho_0 \Delta.
\end{aligned}$$

On writing $\Delta = \frac{\partial v_z}{\partial z}$, we have reduced the hydrodynamic equations to a single second order partial differential equation for v_z,

$$\rho_0 \frac{\partial^2 v_z}{\partial t^2} = c_s^2 \frac{\partial^2 v_z}{\partial z^2} + \gamma g \frac{\partial v_z}{\partial z} \tag{2.69}$$

Following Rae and Roberts (1982), we write

$$Q = \rho_0^{1/2} c_s v_z, \quad \text{or } v_z = Q\, \frac{\rho_0^{-1/2}}{c_s}. \tag{2.70}$$

The new differential components are:

$$\frac{\partial v_z}{\partial t} = \frac{\rho_0^{-1/2}}{c_s} \frac{\partial Q}{\partial t}, \quad \frac{\partial^2 v_z}{\partial t^2} = \frac{\rho_0^{-1/2}}{c_s} \frac{\partial^2 Q}{\partial t^2},$$

and

$$\begin{aligned}
\frac{\partial v_z}{\partial z} &= \frac{\partial}{\partial z}\left[\frac{\rho_0^{-1/2}}{c_s}Q\right] \\
&= \frac{\rho_0^{-1/2}}{c_s}\frac{\partial Q}{\partial z} + Q\frac{d}{dz}\left[\frac{\rho_0^{-1/2}}{c_s}\right] \\
&= \frac{\rho_0^{-1/2}}{c_s}\frac{\partial Q}{\partial z} + Q\frac{d}{dz}\left[\frac{1}{(\gamma p_0)^{1/2}}\right], \qquad c_s^2 = \frac{\gamma p_0}{\rho_0}, \\
&= \frac{\rho_0^{-1/2}}{c_s}\frac{\partial Q}{\partial z} + Q\frac{1}{\gamma^{1/2}}\left(\frac{-1}{2}\right)p_0^{-3/2}p_0' \\
&= \frac{\rho_0^{-1/2}}{c_s}\frac{\partial Q}{\partial z} - \frac{1}{2}Q\frac{1}{(\gamma p_0)^{1/2}}\frac{1}{p_0}\rho_0 g, \qquad p_0' = \rho_0 g, \\
&= \frac{\rho_0^{-1/2}}{c_s}\frac{\partial Q}{\partial z} - \frac{1}{2}Q\frac{\rho_0^{-1/2}}{c_s}\frac{\gamma g}{c_s^2}, \qquad p_0 = \frac{c_s^2\rho_0}{\gamma}.
\end{aligned}$$

In a similar fashion, we may obtain an expression for the second derivative of v_z with respect to z,

$$\frac{\partial^2 v_z}{\partial z^2} = \frac{\rho_0^{-1/2}}{c_s}\frac{\partial^2 Q}{\partial z^2} - \frac{\rho_0^{-1/2}}{c_s}\frac{\gamma g}{c_s^2}\frac{\partial Q}{\partial z} + \frac{3}{4}\frac{\rho_0^{-1/2}}{c_s}\left(\frac{\gamma g}{c_s}\right)^2 Q - \frac{1}{2}\frac{\rho_0^{-1/2}}{c_s}\frac{\gamma g}{c_s^2}\frac{\rho_0'}{\rho_0}Q.$$

Substituting these expressions into the second order partial differential equation (2.69) leads to an ordinary differential equation in Q. The coefficient of $\frac{\partial Q}{\partial z}$ is

$$c_s^2\left[\frac{\rho_0^{-1/2}}{c_s}\frac{\gamma g}{c_s^2}\right] + \gamma g\frac{\rho_0^{-1/2}}{c_s} = 0.$$

The coefficient of Q is given by

$$c_s^2\left[\frac{3}{4}\frac{\rho_0^{-1/2}}{c_s}\frac{\gamma^2 g^2}{c_s^2} - \frac{1}{2}\frac{\rho_0^{-1/2}}{c_s}\frac{\gamma g}{c_s^2}\frac{\rho_0'}{\rho_0}\right] + \gamma g\left[\frac{-1}{2}\frac{\rho_0^{-1/2}}{c_s}\frac{\gamma g}{c_s^2}\right]$$

$$\begin{aligned}
&= \frac{\rho_0^{-1/2}}{c_s}\gamma g\left[\frac{3}{4}\frac{\gamma g}{c_s^2} - \frac{1}{2}\frac{\rho_0'}{\rho_0} - \frac{1}{2}\frac{\gamma g}{c_s^2}\right] \\
&= \frac{\rho_0^{-1/2}}{c_s}\gamma g\left[\frac{1}{4}\frac{\gamma g}{c_s^2} - \frac{1}{2c_s^2}\left(\gamma g - (c_s^2)'\right)\right], \qquad (c_s^2)' = \gamma g - c_s^2\frac{\rho_0'}{\rho_0} \\
&= \frac{\rho_0^{-1/2}}{c_s}\left[\frac{1}{2}\frac{\gamma g}{c_s^2}(c_s^2)' - \frac{1}{4}\frac{\gamma^2 g^2}{c_s^2}\right].
\end{aligned}$$

Thus, overall our equation for Q is

$$\frac{\partial^2 Q}{\partial t^2} - c_s^2 \frac{\partial^2 Q}{\partial z^2} + \Omega^2 Q = 0, \tag{2.71}$$

where

$$\Omega^2 = \frac{1}{4}\frac{\gamma^2 g^2}{c_s^2} - \frac{1}{2}\frac{\gamma g}{c_s^2}\left(c_s^2\right)'. \tag{2.72}$$

Hence, we have obtained the Klein-Gordon equation for the vertical propagation of acoustic waves in the presence of gravity. This result is in agreement with the discussion in Rae and Roberts (1982), who considered an isolated thin flux tube with arbitrary cross-sectional variation. Our result agrees with the more general formula given in Rae and Roberts (1982) when their result is applied to a straight and rigid tube.

Chapter 3

Coronal loop oscillation model

3.1 Coronal Loop model

With this model of a coronal loop we investigate the importance of two effects: gravity, and the addition of a chromospheric layer below the corona. Consider a coronal loop of half-length L with its footpoints of extent h embedded in the chromosphere (see Figure 3.1).

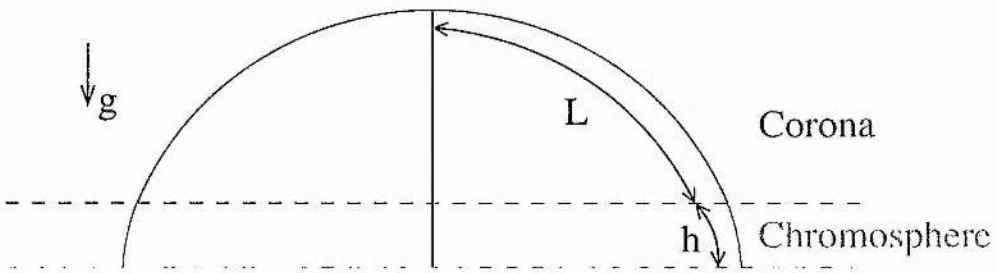

Figure 3.1: Coronal loop of half-length L with chromospheric footpoints of extent h.

Assuming the loop is symmetric about its apex means that only half the loop need be considered. It also simplifies the geometry of the situation so that a cartesian co-ordinate system may be used instead of a cylindrical system. The half loop is straightened out with the z-axis taken along the loop. The apex of the loop is taken to be at $z = 0$ (see Figure 3.2).

To investigate oscillations in such a loop, we consider sound waves propagating vertically in a stratified atmosphere where magnetic effects are ignored. The stratification comes from the consideration of uniform gravity $\mathbf{g} = (0, 0, g)$, aligned with the z-axis. To investigate the role of the two layers, corona and chromosphere, the sound speed is taken to be a function of z. This function, $c_s(z)$, is in general arbitrary. For this work we have considered two cases. The

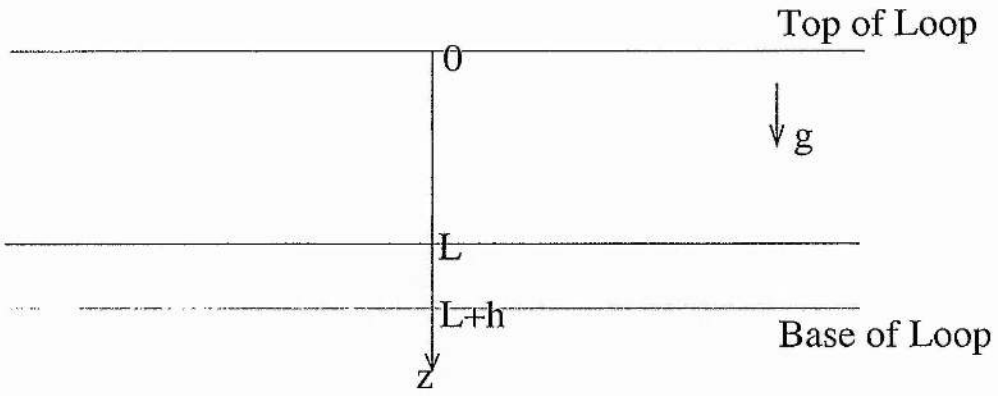

Figure 3.2: Symmetrical coronal loop model aligned with the z-axis, with apex at $z = 0$. Gravity is aligned with the z-axis.

first is a step function

$$c_s(z) = \begin{cases} c_c, & z < L, \\ c_p, & L < z < L + h, \end{cases} \tag{3.1}$$

where c_c denotes the sound speed in the corona and c_p is the value of the sound speed in the chromosphere/photosphere. The second case considers a continuous variation in sound speed,

$$c_s(z) = c_0(1 - \alpha z)^{1/2}; \tag{3.2}$$

the sound speed decreases (at a steady rate determined by α) from a value c_0 at $z = 0$ down through the corona and into the chromosphere.

This setup leads us to consider the linearised hydrodynamic model. As detailed in section 2.9, this model leads to the Klein-Gordon equation for Q,

$$Q(z,t) = \rho_0^{1/2}(z)c_s(z)v_z(z,t), \tag{3.3}$$

namely,

$$\frac{\partial^2 Q}{\partial t^2} - c_s^2\frac{\partial^2 Q}{\partial z^2} + \Omega^2 Q = 0, \tag{3.4}$$

where

$$\Omega^2 = \frac{1}{4}\frac{\gamma^2 g^2}{c_s^2} - \frac{1}{2}\frac{\gamma g}{c_s^2}\left(c_s^2\right)'. \tag{3.5}$$

Here a dash $'$ denotes differentiation with respect to z.

We note that in the special case of zero gravity, we recover pure sound waves (section 2.2): with $\Omega^2 = 0$, the Klein-Gordon equation (3.4) reduces to

$$\frac{\partial^2 Q}{\partial t^2} = c_s^2 \frac{\partial^2 Q}{\partial z^2}, \tag{3.6}$$

which is the one dimensional wave equation with propagation speed c_s.

Returning to the Klein-Gordon equation (3.4), with $\Omega \neq 0$ and taking a Fourier component in t, $Q \propto e^{i\omega t}$, where ω is the wave frequency, we find that (3.4) reduces to the ordinary differential equation,

$$\frac{d^2 Q}{dz^2} + k^2(z) Q = 0, \tag{3.7}$$

where

$$k^2(z) = \begin{cases} k_c^2 = \frac{\omega^2 - \Omega_c^2}{c_c^2}, & 0 < z < L, \\ k_p^2 = \frac{\omega^2 - \Omega_p^2}{c_p^2}, & L < z < L + h. \end{cases} \tag{3.8}$$

3.2 Case 1 - Isothermal atmosphere

Taking the step function form of the sound speed (equation (3.1)) is equivalent to considering the corona and chromosphere each as distinct isothermal atmospheres. Under isothermal conditions the sound speed is constant and Ω^2 reduces to

$$\Omega^2 = \frac{1}{4} \frac{\gamma^2 g^2}{c_s^2}. \tag{3.9}$$

Thus we obtain the cut-off frequency $\Omega = \gamma g / 2 c_s$ first considered by Lamb (1909, 1932).

3.2.1 Dispersion relation

In these circumstances a trigonometrical solution of the ordinary differential equation (3.7) exists, namely

$$Q = \begin{cases} A_1 \cos k_c z + B_1 \sin k_c z, & 0 < z < L, \\ A_2 \cos k_p z + B_2 \sin k_p z, & L < z < L + h, \end{cases} \tag{3.10}$$

where A_1, A_2, B_1 and B_2 are constants and $k_{c,p}^2$ are given by equation (3.8).

Since there are four constants (A_1, A_2, B_1 and B_2), four boundary conditions are required. We impose zero velocity at the loop summit ($z = 0$) and

at the loop footpoint $z = L + h$.

The condition $v_z = 0$ at the loop apex is chosen for convenience; we are assuming that the oscillations have a node at the summit of the loop. Alternatively, we may consider that $v_z' = 0$ at the loop summit. The condition $z_z = 0$ at $z = L + h$ means that there is no vertical motion at the loop footpoint; this condition is chosen to reflect the line-tying effect of the dense chromosphere on any motions generated within the corona. The equilibrium density $\rho_0(z)$ varies exponentially but since $Q = \rho_0^{1/2} c_s v_z$, the requirement that $v_z = 0$ at $z = 0$ and $z = L + h$ means that

$$Q = 0 \text{ at } z = 0 \text{ and } z = L + h. \tag{3.11}$$

The model must be consistent across the boundary between the corona and the chromospheric base. The velocity, v_z, must be continuous at the interface $z = L$. In view of the relation $c_s^2 = \gamma p_0/\rho_0$ (equation 2.12), giving

$$Q = \left(\rho_0 c_s^2\right)^{1/2} v_z = \left(\gamma p_0\right)^{1/2} v_z,$$

and the fact that the equilibrium pressure of $p_0(z)$ is continuous, continuity of v_z implies

$$Q \text{ is continuous across } z = L. \tag{3.12}$$

Our fourth boundary condition is found by considering the integration of the differential equation (3.7) over a small neighbourhood of $z = L$. The details of this calculation are given in Appendix A, and lead to the condition that

$$\frac{dQ}{dz} - \frac{1}{2\Lambda_0} Q \text{ is continuous across } z = L; \tag{3.13}$$

here $\Lambda_0(z)$ is the pressure scale height related to the sound speed by

$$c_s^2 = \gamma g \Lambda_0. \tag{3.14}$$

The boundary conditions (3.11) at $z = 0$ and $z = L + h$ reduce Q to

$$Q = \begin{cases} B_1 \sin k_c z, & 0 < z < L, \\ B_2 \sin k_p (z - (L + h)), & L < z < L + h. \end{cases} \tag{3.15}$$

At $z = L$, the two boundary conditions (3.12) and (3.13) give:

$$B_1 \sin k_c L = B_2 \sin k_p(-h),$$
$$k_c B_1 \cos k_c L - \frac{1}{2\Lambda_c} B_1 \sin k_c L = k_p B_2 \cos k_p(-h) - \frac{1}{2\Lambda_p} B_2 \sin k_p(-h).$$

The condition for a non-zero solution of these two equations for B_1 and B_2 is that the determinant of the coefficients must be zero:

$$\begin{vmatrix} \sin k_c L & \sin k_p h \\ k_c \cos k_c L - \frac{1}{2\Lambda_c} \sin k_c L & -k_p \cos k_p h - \frac{1}{2\Lambda_p} \sin k_p h \end{vmatrix} = 0. \qquad (3.16)$$

Expansion of the determinant (3.16) results in the required dispersion relation for a two-layer system stratified by gravity,

$$\left(\frac{1}{2\Lambda_c} - \frac{1}{2\Lambda_p}\right) \sin k_c L \sin k_p h - k_p \sin k_c L \cos k_p h - \\ - k_c \sin k_p h \cos k_c L = 0. \qquad (3.17)$$

The wavenumbers k_c and k_p are defined in equation (3.8).

3.2.2 An isolated medium

To understand the dispersion relation (3.17), we can check that when taking the limits $h \to 0$ or $L \to 0$ the expected result is obtained. The expected result is found by considering a solution of the ordinary differential equation (3.7) in an infinitely wide, isolated slab of height L when k is constant, so that the chromospheric layer is ignored (see Figure 3.3).

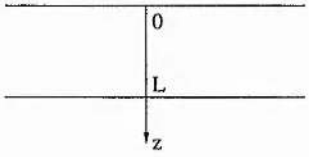

Figure 3.3: A coronal region of extent L, bounded at $z = 0$ and $z = L$.

Again the differential equation (3.7) has a trigonometrical solution, namely,

$$Q = A \cos k_c z + B \sin k_c z,$$

where A, B are constants. In order to compare a resulting dispersion relation with the full dispersion relation (3.17), the same boundary conditions must be

used. Thus imposing $v_z = Q = 0$ at $z = 0$ reduces Q to

$$Q = B \sin k_c z.$$

Imposing $Q = 0$ at $z = L$ gives

$$\sin k_c L = 0. \tag{3.18}$$

Thus,

$$k_c = \frac{n\pi}{L}, \qquad n = 1, 2, 3, ... \tag{3.19}$$

Expanding k_c in terms of ω, using the coronal part of equation (3.8), gives

$$\omega^2 = \frac{n^2\pi^2}{L^2}\, c_c^2 + \Omega_c^2. \tag{3.20}$$

Now consider the full dispersion relation (3.17) under the limit $h \to 0$, implying that $\sin k_p h \to 0$ and $\cos k_p h \to 1$. The reduced dispersion relation is

$$\sin k_c L = 0. \tag{3.21}$$

Thus we recover $k_c L = n\pi$.

A similar solution is found when considering propagation of sound waves in a purely chromospheric layer, obtained by taking the limit $L \to 0$. In this case the dispersion relation (3.17) reduces to

$$\sin k_p h = 0. \tag{3.22}$$

Thus $k_p h = n\pi$; using the chromospheric part of equation (3.8) leads to the result

$$\omega^2 = \frac{n^2\pi^2}{h^2}\, c_p^2 + \Omega_p^2. \tag{3.23}$$

3.2.3 Shallow chromospheric layer

Physically, the chromosphere contains only a small percentage of the total length of a coronal loop though by contrast it may contain a greater mass, because of the higher plasma density. It is interesting to consider the limiting case $h \ll L$, or $k_p h \ll 1$. In the case $k_p h \ll 1$ the trigonometric terms in the

dispersion relation may be expanded:

$$\sin k_p h \approx k_p h \left[1 - O(k_p^2 h^2)\right],$$
$$\cos k_p h \approx 1 - O(k_p^2 h^2).$$

Using these expressions, the general dispersion relation (3.17) reduces to

$$\frac{1}{2}\left(\frac{1}{\Lambda_c} - \frac{1}{\Lambda_p}\right) k_p h \, \sin k_c L - k_p \sin k_c L - k_p h \, k_c \cos k_c L = 0. \tag{3.24}$$

This reduced dispersion relation can be rewritten in the form

$$\sin k_c L = \epsilon f\left(k_c L\right), \tag{3.25}$$

where $\epsilon = k_p h \ll 1$. To achieve this we divide equation (3.24) by k_p. It is useful to restrict the occurrences of k_c to the combination $k_c L$, so we also multiply the equation by L. Thus,

$$\sin k_c L = \frac{1}{k_p L} k_p h \left[\frac{L}{2}\left(\frac{1}{\Lambda_c} - \frac{1}{\Lambda_p}\right) \sin k_c L - k_c L \cos k_c L\right], \tag{3.26}$$

so that

$$f(k_c L) = \frac{1}{2k_p}\left(\frac{1}{\Lambda_c} - \frac{1}{\Lambda_p}\right) \sin k_c L - \frac{1}{k_p L} k_c L \cos k_c L. \tag{3.27}$$

Since ϵ is small, we consider the limit $\epsilon \to 0$. This reduces the situation to simply $\sin k_c L = 0$, or $k_c L = n\pi$, with $n = 1, 2, \ldots$. Since we are looking at $\sin k_c L = \epsilon f(k_c L)$, where ϵ is small, we may write

$$k_c L = n\pi + \epsilon \, C_n, \tag{3.28}$$

for some constants C_n.

By calculating $\sin(n\pi + \epsilon C_n)$ and $\cos(n\pi + \epsilon C_n)$, an expression for $f(k_c L)$ in terms of C_n can be found:

$$\begin{aligned}
\sin(n\pi + \epsilon C_n) &= \sin n\pi \, \cos \epsilon C_n + \cos n\pi \, \sin \epsilon C_n \\
&= 0 \times \cos \epsilon C_n + (-1)^n \epsilon C_n (1 - O(\epsilon^2 C_n^2)) \\
&\approx (-1)^n \epsilon C_n
\end{aligned} \tag{3.29}$$

$$\begin{aligned}
\cos(n\pi + \epsilon C_n) &= \cos n\pi \, \cos \epsilon C_n - \sin n\pi \, \cos \epsilon C_n \\
&= (-1)^n (1 - O(\epsilon^2 C_n^2) - 0 \times \cos \epsilon C_n \\
&\approx (-1)^n.
\end{aligned} \tag{3.30}$$

Substituting (3.29) and (3.30) into $f(k_cL)$ (equation 3.27) gives

$$f(n\pi + \epsilon C_n) = \frac{1}{2k_p}\left(\frac{1}{\Lambda_c} - \frac{1}{\Lambda_p}\right)(-1)^n \epsilon C_n - \frac{1}{k_pL}(n\pi + \epsilon C_n)(-1)^n. \quad (3.31)$$

By substituting this expression for $f(k_cL)$ into equation (3.26) we obtain C_n,

$$\begin{aligned}
\sin(n\pi + \epsilon C_n) &= \epsilon f(n\pi + \epsilon C_n), \\
(-1)^n\,\epsilon\,C_n &= \epsilon\left[\frac{1}{2k_p}\left(\frac{1}{\Lambda_c} - \frac{1}{\Lambda_p}\right)(-1)^n\,\epsilon\,C_n - \frac{1}{k_pL}\,(n\pi + \epsilon\,C_n)(-1)^n\right], \\
&= -\frac{n\pi\epsilon(-1)^n}{k_pL},
\end{aligned}$$

to first order. Hence,

$$C_n = -\frac{n\pi}{k_pL}. \quad (3.32)$$

We now have a solution, k_cL, of the dispersion relation for wave propagation in the limiting case $k_ph \ll 1$, namely

$$\begin{aligned}
k_cL &= n\pi + \epsilon C_n, \\
&= n\pi\left(1 - \frac{h}{L}\right). \quad (3.33)
\end{aligned}$$

Since $k_c^2 = (\omega^2 - \Omega_c^2)/c_c^2$, this leads to the solution

$$\omega^2 = \Omega^2 + \frac{c_c^2}{L^2}(k_cL)^2 = \Omega^2 + \frac{n^2\pi^2c_c^2}{L^2}\left(1 - \frac{h}{L}\right)^2; \quad (3.34)$$

that is,

$$\omega^2 = \Omega^2 + \frac{n^2\pi^2c_c^2}{L^2}\left(1 - \frac{2h}{L}\right). \quad (3.35)$$

In the case $k_ph \ll 1$, the frequency of sound waves propagating in a coronal atmosphere has a cut off frequency of $\left(\Omega^2 + \frac{n^2\pi^2c_c^2}{L^2}\right)^{1/2}$.

3.2.4 Dimensionless dispersion relation

For numerical treatment of the full dispersion relation we write it in dimensionless form. This is easily achieved by multiplying the equation by Λ_c:

$$\frac{1}{2}\left(1-\frac{\Lambda_c}{\Lambda_p}\right)\sin k_c L \sin k_p h - k_p\Lambda_c \sin k_c L \cos k_p h - \\ - k_c\Lambda_c \sin k_p h \cos k_c L = 0. \quad (3.36)$$

The wave frequency ω enters through the wavenumbers k_c and k_p defined in equation (3.8). We rewrite the dispersion relation so that ω is more explicit. Set

$$\overline{\omega} = \frac{\omega}{\Omega_c}, \quad (3.37)$$

a dimensionless measure of the frequency ω. It is convenient to express $k_p\Lambda_c$, $k_c\Lambda_c$, $k_c L$ and $k_p h$ in terms of $\overline{\omega}$ and the parameters

$$r = \frac{\Lambda_p}{\Lambda_c} = \frac{c_p^2}{c_c^2}, \quad s = \frac{L}{\Lambda_c}, \quad \text{and} \quad \zeta = \frac{h}{\Lambda_c}. \quad (3.38)$$

As shown in Appendix B, the dimensionless dispersion relation describing wave propagation in a two-layer system stratified by gravity is

$$\frac{1}{2}(1-r)\sin\left(\frac{s^2}{4}\left(\overline{\omega}^2-1\right)\right)^{1/2}\sin\left(\frac{\zeta^2}{4r}\left(\overline{\omega}^2-\frac{1}{r}\right)\right)^{1/2} \\ -\left(\frac{1}{4r}\left(\overline{\omega}^2-\frac{1}{r}\right)\right)^{1/2}\sin\left(\frac{s^2}{4}\left(\overline{\omega}^2-1\right)\right)^{1/2}\cos\left(\frac{\zeta^2}{4r}\left(\overline{\omega}^2-\frac{1}{r}\right)\right)^{1/2} \\ -\left(\frac{1}{4}\left(\overline{\omega}^2-1\right)\right)^{1/2}\sin\left(\frac{\zeta^2}{4r}\left(\overline{\omega}^2-\frac{1}{r}\right)\right)^{1/2}\cos\left(\frac{s^2}{4}\left(\overline{\omega}^2-1\right)\right)^{1/2} = 0. \quad (3.39)$$

The three new parameters r, s, and ζ have meaning in terms of the model. The constant r shows the relation between the corona and the chromospheric layer, using as a measure the relative squared sound speeds, c_c^2 and c_p^2 (or, equivalently, the pressure scale heights Λ_c and Λ_p). The parameter ζ is a measure of the chromospheric extent. Finally, s is a measure of the length of the loop and consequently varies from loop to loop.

For a typical coronal temperature of 10^6K and a chromospheric temperature of 10^4K, we can determine the corresponding pressure scale heights and

sound speeds (see Appendix C for the details) obtaining

$$\Lambda_c \approx 5 \times 10^4 \text{ km}, \qquad \Lambda_p \approx 500 \text{ km} \tag{3.40}$$

and

$$c_c \approx 152 \text{ km s}^{-1}, \qquad c_p \approx 15 \text{ km s}^{-1}. \tag{3.41}$$

Using these values we can calculate a value for the fraction r,

$$r = \frac{\Lambda_p}{\Lambda_c} = \frac{1.4 \times 10^5 \text{m}}{5 \times 10^7 \text{m}} \approx \frac{1}{300}. \tag{3.42}$$

The extent of the chromosphere is very small compared to the radius of the Sun, but the actual value is unclear. Values ranging from 1000 km [2] to 2500 km (Lang 2001), or even up to 10000 km (Golub and Pasachoff 2001) are suggested. However, since the pressure scale height in the corona is of the order 10^4km, this tells us that generally $\beta \ll 1$.

The average loop length observed by TRACE in the corona is 110 Mm (Aschwanden *et al.* 2002). This gives an average value of s of about 10. In general we consider short loops to have $s \ll 1$ and long loops to have $s \gg 1$. We can use this definition of 'short' and 'long' to analyse further the dispersion relation for wave propagation in an isolated coronal atmosphere (section 3.2.2). We found the dispersion relation to be

$$\omega^2 = \frac{n^2\pi^2 c_c^2}{L^2} + \Omega_c^2,$$

that is,

$$\frac{\omega^2}{\Omega_c^2} = 1 + \frac{n^2\pi^2}{L^2}\frac{c_c^2}{\Omega_c^2} = 1 + \frac{n^2\pi^2}{L^2}\frac{\gamma g \Lambda_c}{\frac{1}{4}\gamma g}.$$

In terms of the dimensionless variables $\overline{\omega}$ and s,

$$\overline{\omega}^2 = 1 + \frac{4n^2\pi^2}{s^2}. \tag{3.43}$$

For a short ($s \to 0$) loop, $\overline{\omega}^2 \to \infty$; for a long ($s \to \infty$) loop, $\overline{\omega}^2 \to 1$, i.e.

$$\omega \approx \Omega_c. \tag{3.44}$$

This is illustrated in Figure 3.4. This simple analysis also provides us with an idea of how the period $\tau (= 2\pi/\omega)$ of such waves will change with loop length

L (see Figure 3.5). The period τ of an oscillation lies below $2\pi/\Omega_c$.

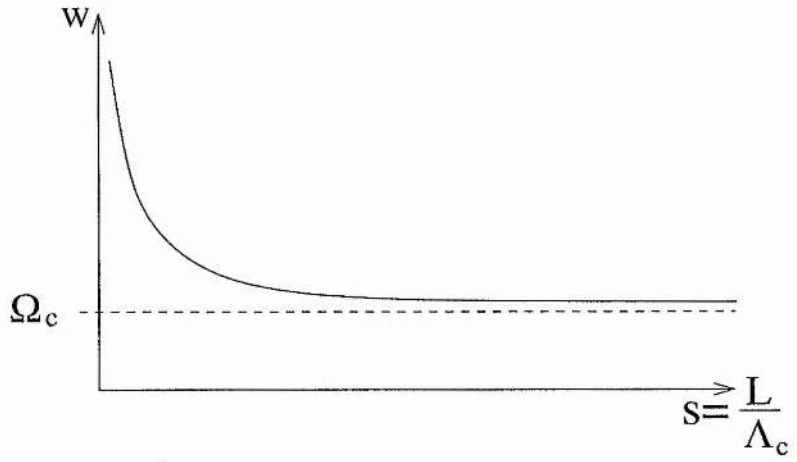

Figure 3.4: Sketch of the dimensionless wave frequency $\overline{\omega}(= \omega/\Omega_c)$ against $s = L/\Lambda_c$ for an isolated coronal structure, showing a cut-off frequency Ω_c.

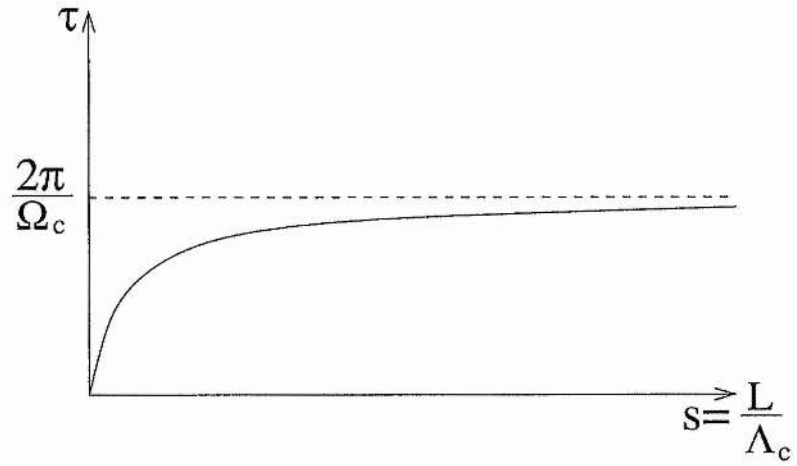

Figure 3.5: Sketch of the period $\tau(= 2\pi/\omega)$ against dimensionless loop length $s = L/\Lambda_c$ for an isolated coronal structure, showing a maximum period of $2\pi/\Omega_c$.

3.3 Case 2 - Continuous sound speed

We return to the Klein-Gordon Equation

$$\frac{\partial^2 Q}{\partial t^2} - c_s^2 \frac{\partial^2 Q}{\partial z^2} + \Omega^2 Q = 0, \qquad Q = (\rho_0 c_s)^{1/2} v_z,$$

where

$$\Omega^2 = \frac{1}{4}\frac{\gamma^2 g^2}{c_s^2} - \frac{1}{2}\frac{\gamma g}{c_s^2}(c_s^2)'.$$

In section 3.2 we took the sound speed to be a step function with c_s taking different constant values in the coronal and chromospheric layers. Here we consider the continuous function

$$c_s = c_0(1 - \alpha z)^{1/2}, \quad z > 0, \tag{3.45}$$

where α (¿0) is a constant so that the sound speed squared decreases from a value $c_s^2 = c_0^2$ at the loop apex ($z = 0$), through the corona and into the chromospheric layer, at a constant rate α. With this form of the sound speed, Ω^2 becomes

$$\Omega^2 = \frac{1}{4}\frac{\gamma^2 g^2}{c_0^2}\frac{1}{(1-\alpha z)} + \frac{1}{2}\frac{\gamma g \alpha}{(1-\alpha z)}. \tag{3.46}$$

Taking a Fourier component in t, so that $Q \propto \exp i\omega t$, reduces the Klein-Gordon equation from a partial differential equation to an ordinary differential equation, namely

$$\frac{d^2 Q}{dz^2} + \left(\frac{\omega^2 - \Omega^2(z)}{c_s^2(z)}\right) Q = 0. \tag{3.47}$$

The presence of the combination $(1 - \alpha z)$, in both $\Omega^2(z)$ and $c_s^2(z)$, suggests a suitable change of variable. We write

$$u = 1 - \alpha z. \tag{3.48}$$

In order to make this change of variable we need to find the differential operators:

$$\frac{d}{dz} = \frac{d}{du}\left(\frac{du}{dz}\right) = -\alpha\frac{d}{du},$$
$$\frac{d^2}{dz^2} = \frac{d}{dz}\cdot\frac{d}{dz} = \left(-\alpha\frac{d}{du}\right)\left(-\alpha\frac{d}{du}\right) = \alpha^2\frac{d^2}{dz^2};$$

also,

$$\Omega^2 = \frac{1}{u}\left[\frac{\gamma^2 g^2}{4c_0^2} + \frac{\gamma g \alpha}{2}\right] = \frac{1}{u}\beta_0,$$

where

$$\beta_0 = \frac{\gamma^2 g^2}{4c_0^2} + \frac{\gamma g \alpha}{2}. \tag{3.49}$$

Equation (3.47) becomes a differential equation in u, namely,

$$u\frac{d^2Q}{du^2} + \left[\frac{\omega^2}{\alpha^2 c_0^2} - \frac{\beta_0}{\alpha^2 c_0^2}\frac{1}{u}\right]Q = 0,$$

that is,

$$\frac{d^2Q}{du^2} + \left[\frac{\omega^2}{\alpha^2 c_0^2}\frac{1}{u} - \frac{\beta_0}{\alpha^2 c_0^2}\frac{1}{u^2}\right]Q = 0 \tag{3.50}$$

This is a form of Bessel's equation with a known solution. In Abramowitz and Stegun (1964; section 9.1.50), we have the result:

$$w'' + \left(\frac{\lambda^2}{4z} - \frac{\nu^2 - 1}{4z^2}\right)w = 0 \tag{3.51}$$

has solution

$$w = z^{1/2}\mathcal{C}_\nu(\lambda z^{1/2}), \tag{3.52}$$

where $\mathcal{C}_\nu$ is either of the standard Bessel functions $\mathcal{J}_\nu$ and $\mathcal{Y}_\nu$ of order ν. Applied to equation (3.50),

$$\frac{\lambda^2}{4} = \frac{\omega^2}{\alpha^2 c_0^2}, \qquad \lambda = \frac{2\omega}{\alpha c_0}, \tag{3.53}$$

$$\frac{\nu^2 - 1}{4} = \frac{\beta_0}{\alpha^2 c_0^2}, \qquad \nu = \left(\frac{4\beta_0}{\alpha^2 c_0^2} + 1\right)^{1/2}. \tag{3.54}$$

Hence a solution of (3.50) is

$$Q = (1 - \alpha z)^{1/2}\mathcal{C}_\nu\left(\frac{2\omega}{\alpha c_0}(1 - \alpha z)^{1/2}\right), \tag{3.55}$$

where ν is given as above. The form of ν appears quite complicated; however, on substitution of β_0 we obtain

$$\begin{aligned}\nu^2 &= \frac{4}{\alpha^2 c_0^2}\left(\frac{\gamma^2 g^2}{4c_0^2} + \frac{\gamma g \alpha}{2}\right) + 1 \\ &= \frac{\gamma^2 g^2}{\alpha^2 c_0^4} + \frac{2\gamma g}{\alpha c_0^2} + 1 = \left(\frac{\gamma g}{\alpha c_0^2} + 1\right)^2.\end{aligned}$$

Hence,

$$\nu = 1 + \frac{\gamma g}{\alpha c_0^2}. \tag{3.56}$$

3.3.1 Confirming the Bessel result

We can confirm this result by finding a standard Bessel equation (Abramowitz and Stegun 1964) of the form

$$z^2 \frac{d^2 Q}{dz^2} + z\frac{dQ}{dz} + (z^2 - \nu^2)Q = 0. \tag{3.57}$$

With a little foresight we know we can take a factor of $(1 - \alpha z)^{1/2}$ from the solution. Write $Q(u) = u^{1/2}R(u)$, where $u = 1 - \alpha z$ as before, and find the differential operators,

$$\begin{aligned}\frac{dQ}{du} &= \frac{d}{du}\left(u^{1/2}R\right) = u^{1/2}\frac{dR}{du} + \frac{1}{2}u^{-1/2}R, \\ \frac{d^2Q}{du^2} &= \frac{d}{du}\left(\frac{dQ}{du}\right) = \frac{d}{du}\left[u^{1/2}\frac{dR}{du} + \frac{1}{2}u^{-1/2}R\right] \\ &= u^{1/2}\frac{d^2R}{du^2} + u^{-1/2}\frac{dR}{du} - \frac{1}{4}u^{-3/2}R.\end{aligned}$$

Substituting these differential operators in the differential equation (3.50) for Q in terms of u leads to a differential equation for R:

$$u^2\frac{d^2R}{du^2} + u\frac{dR}{du} + \left[u\frac{\omega^2}{\alpha^2 c_0^2} - \left(\frac{\beta_0}{\alpha^2 c_0^2} + \frac{1}{4}\right)\right]R = 0. \tag{3.58}$$

We then write $u = y^2$, which has differential operators,

$$\begin{aligned}\frac{d}{du} &= \frac{d}{dy}\frac{dy}{du} = \frac{1}{2}u^{-1/2}\frac{d}{dy} = \frac{1}{2y}\frac{d}{dy}, \\ \frac{d^2}{du^2} &= \frac{d}{du}\frac{d}{du} = \left(\frac{1}{2y}\frac{d}{dy}\right)\left(\frac{1}{2y}\frac{d}{dy}\right) \\ &= \frac{1}{4y^2}\frac{d^2}{dy^2} - \frac{1}{4y^3}\frac{d}{dy}.\end{aligned}$$

This substitution changes the differential equation (3.58) for R in terms of u, to a differential equation for R in terms of y:

$$y^2\frac{d^2R}{dy^2} + \frac{y}{4}\frac{dR}{dy} + \left[A^2y^2 - \nu^2\right]R = 0, \tag{3.59}$$

where,

$$A^2 = \frac{4\omega^2}{\alpha^2 c_0^2}, \quad \nu^2 = \frac{4\beta_0}{\alpha^2 c_0^2} + 1. \tag{3.60}$$

Finally, letting $\hat{y} = Ay$, so that

$$\frac{d}{dy} = A\frac{d}{d\hat{y}}, \quad \frac{d^2}{dy^2} = A^2\frac{d^2}{d\hat{y}^2},$$

changes the differential equation (3.59) for R in terms of y to a differential equation for R in terms of $\hat{y}$:

$$\hat{y}\frac{d^2R}{d\hat{y}^2} + \hat{y}\frac{dR}{d\hat{y}} + \left[\hat{y}^2 - \nu^2\right]R = 0. \tag{3.61}$$

This has the form of the standard Bessel equation (3.57) with solution a Bessel function of order ν,

$$R = C_\nu(\hat{y}), \quad Qu^{-1/2} = C_\nu(Ay)$$

Thus,

$$Q = (1-\alpha z)^{1/2} C_\nu\left(\frac{2\omega}{\alpha c_o}(1-\alpha z)^{1/2}\right), \tag{3.62}$$

where ν is given by equation (3.56).

3.3.2 Dispersion relation

Before finding a dispersion relation by applying boundary conditions, we consider how $(1-\alpha z)^{1/2}$ may be rewritten. The factor $(1-\alpha z)$ appears in the equations for the sound speed, so that

$$(1-\alpha z)^{1/2} = \frac{c_s(z)}{c_0}. \tag{3.63}$$

Using this form, the general solution of the Bessel equation is

$$Q = C_1 c_s(z)\mathcal{J}_\nu\left(\frac{2\omega}{\alpha c_0}\frac{c_s(z)}{c_0}\right) + C_2 c_s(z)\mathcal{Y}_\nu\left(\frac{2\omega}{\alpha c_0}\frac{c_s(z)}{c_0}\right), \tag{3.64}$$

where C_1 and C_2 are constants and $1/c_0$ has been incorporated into these two constants. With two constants we require two boundary conditions. We apply the same conditions at the loop apex and footpoint as previously with a step function sound-speed, i.e. zero velocity at $z = 0$ and at $z = L + h$. Applying $Q = 0$ at $z = 0$ gives

$$C_1 \mathcal{J}_\nu \left(\frac{2\omega}{\alpha c_o} \right) + C_2 \mathcal{Y}_\nu \left(\frac{2\omega}{\alpha c_o} \right) = 0. \tag{3.65}$$

Applying $Q = 0$ on $z = L + h$ gives

$$C_1 \mathcal{J}_\nu \left(\frac{2\omega}{\alpha c_o} \frac{c_{base}}{c_0} \right) + C_2 \mathcal{Y}_\nu \left(\frac{2\omega}{\alpha c_o} \frac{c_{base}}{c_0} \right) = 0, \tag{3.66}$$

where c_{base} is the value of the sound speed at the base of the loop $z = L + h$. It is important to remember that α is present in this equation for

$$c_{base} = c_0(1 - \alpha(L + h))^{1/2}. \tag{3.67}$$

To ensure a non-zero solution of equations (3.65) and (3.66), the determinant of the coefficients must be zero,

$$\begin{vmatrix} \mathcal{J}_\nu \left(\frac{2\omega}{\alpha c_o} \right) & \mathcal{Y}_\nu \left(\frac{2\omega}{\alpha c_o} \right) \\ \mathcal{J}_\nu \left(\frac{2\omega}{\alpha c_o} \frac{c_{base}}{c_0} \right) & \mathcal{Y}_\nu \left(\frac{2\omega}{\alpha c_o} \frac{c_{base}}{c_0} \right) \end{vmatrix} = 0.$$

Thus,

$$\mathcal{J}_\nu \left(\frac{2\omega}{\alpha c_o} \right) \mathcal{Y}_\nu \left(\frac{2\omega}{\alpha c_o} \frac{c_{base}}{c_0} \right) - \mathcal{J}_\nu \left(\frac{2\omega}{\alpha c_o} \frac{c_{base}}{c_0} \right) \mathcal{Y}_\nu \left(\frac{2\omega}{\alpha c_o} \right) = 0, \tag{3.68}$$

which is the dispersion relation for wave propagation in a medium where the sound speed squared decreases at a constant rate α from a maximum at $z = 0$ to a base at $z = L + h$.

Abramowitz and Stegun (1964) state that the relation

$$\mathcal{J}_\nu(z)\mathcal{Y}_\nu(\lambda z) - \mathcal{Y}_\nu(z)\mathcal{J}_\nu(\lambda z) = 0, \tag{3.69}$$

has solutions for $\lambda > 1$ which may be expressed in asymptotic form. To apply this result to our dispersion relation, we write

$$z = \frac{c_{base}}{c_0} \frac{2\omega}{\alpha c_o}, \qquad \lambda = \frac{c_0}{c_{base}}. \tag{3.70}$$

Then $\lambda > 1$, since c_0 is the maximum value of the sound speed in $0 < z < L + h$.

The asymptotic expansion of the sth zero is (Abramowitz and Stegun 1964)

$$z = \beta + \frac{p}{\beta} + \frac{q - p^2}{\beta^3} + \frac{r - 4pq + 2p^3}{\beta^5} + ... \tag{3.71}$$

where β, p, q, r are given as in Appendix D. Using $c_s(0) = 150$ kms^{-1}, $c_s(L + h) = 15$ kms^{-1}, so that $\lambda = 10$, we can determine numerically the constants α, ν, μ, β, p, q and r. The result is an equation for z,

$$z = \frac{s\pi}{9} + \frac{4.02}{s\pi} - \frac{57.112}{s^3\pi^3} - \frac{83046.78}{s^5\pi^5} + ... \tag{3.72}$$

(see Appendix D for details). The results obtained from this asymptotic solution, and the resulting frequency ω and period τ (in seconds) of such waves is given in Table 3.1.

s	z	ω	τ (secs)
3	0.2887	0.00217	2901
4	1.4224	0.0107	589
5	1.8997	0.0142	441
6	2.2642	0.0170	370
7	2.6047	0.0195	322

Table 3.1: The table shows the frequency ω (s^{-1}) and period $\tau(= 2\pi/\omega)$ for asymptotic solutions ($s = 3..7$) of the Bessel dispersion relation (3.68).

The results here appear to show that the Bessel equation is a possible solution for describing the wave modes. However, the values of z for increasing values of s are not converging. In the next chapter when considering the dispersion equation found in this chapter and analysing the impact of the chromospheric layer and of gravity, we do not use the Bessel results found here.

Chapter 4

Results

In this chapter we consider the importance of the two effects, gravity and the addition of a chromospheric layer below the corona, on the wave oscillations in a coronal loop. We also look at applying this model to results from the SUMER satellite as described by Wang *et al.* (2002, 2003).

4.1 Effect of chromospheric layer

4.1.1 Checking numerical method

To explore the effect of the chromospheric layer we consider the dispersion relation found for an isothermal atmosphere in a coronal loop with its footpoints embedded in the chromosphere,

$$\begin{aligned}
&\frac{1}{2}(1-r)\sin\left(\frac{s^2}{4}\left(\overline{\omega}^2-1\right)\right)^{1/2}\sin\left(\frac{\zeta^2}{4r}\left(\overline{\omega}^2-\frac{1}{r}\right)\right)^{1/2}\\
&-\left(\frac{1}{4r}\left(\overline{\omega}^2-\frac{1}{r}\right)\right)^{1/2}\sin\left(\frac{s^2}{4}\left(\overline{\omega}^2-1\right)\right)^{1/2}\cos\left(\frac{\zeta^2}{4r}\left(\overline{\omega}^2-\frac{1}{r}\right)\right)^{1/2}\\
&-\left(\frac{1}{4}\left(\overline{\omega}^2-1\right)\right)^{1/2}\sin\left(\frac{\zeta^2}{4r}\left(\overline{\omega}^2-\frac{1}{r}\right)\right)^{1/2}\cos\left(\frac{s^2}{4}\left(\overline{\omega}^2-1\right)\right)^{1/2}=0.
\end{aligned} \tag{4.1}$$

We consider (4.1) numerically. We use a simple bisection method to find roots $\overline{\omega}$ for given h and L. This process is repeated for various L, producing dispersion diagrams illustrating how the frequency changes as the loop length increases. To check that the program is working correctly we compare numerical results for small h/Λ_c with those expected from an analytical analysis of the limit $h \to 0$.

For an isolated slab of extent L we found a dimensionless dispersion re-

lation, for $n = 1$:

$$\overline{\omega} = \left(1 + \frac{4\pi^2}{s^2}\right)^{1/2}, \qquad s = \frac{L}{\Lambda_c}. \tag{4.2}$$

Writing $L = \lambda \times 10^8$m, s reduces to the simple form $s = 2\lambda$, which in turn reduces $\overline{\omega}$,

$$\overline{\omega} = \left(1 + \frac{\pi^2}{\lambda^2}\right)^{1/2}. \tag{4.3}$$

Loop length (m)	$\overline{\omega}$ numerical	$\overline{\omega}$ analytical
$L_{min} = 4 \times 10^7$	7.9174	7.9174
$L_{ave} = 1.1 \times 10^8$	3.0248	3.0260
$L_{max} = 2.46 \times 10^8$	1.6232	1.6220

Table 4.1: Comparison of wave frequency $\overline{\omega}$ obtained numerically and analytically for three loop lengths.

Table 4.1 shows the values of $\overline{\omega}$ determined numerically from dispersion relation (4.1) for $h = 10$m, and which we compare with equation (4.3). Three loop lengths are considered which correspond to the minimum, average and maximum loop length reported by Aschwanden *et al.* (2002).

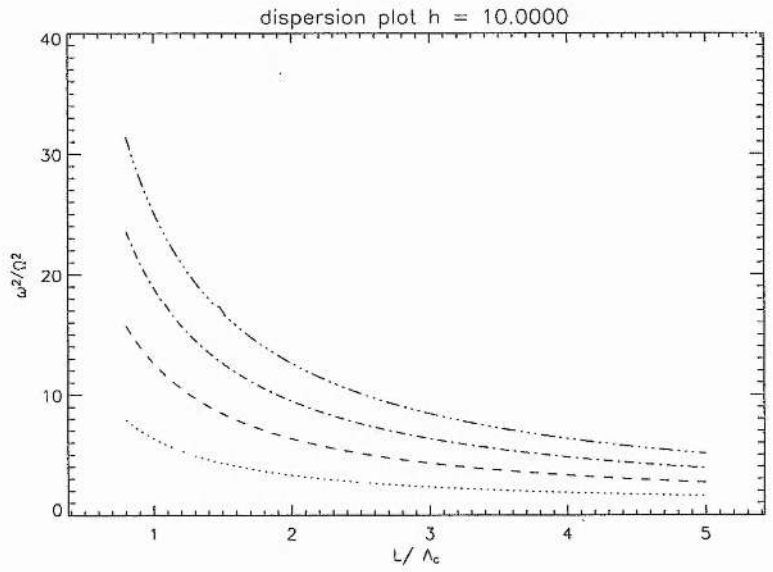

Figure 4.1: Dispersion plot of $\overline{\omega}$ for the first four wave modes ($n = 1, 2, 3, 4$) for small h ($h = 10$ m) showing decreasing frequency as L increases.

The table shows that the numerical method works well for small h, suggesting that results can be trusted for increasing h. The wave frequency decreases as the loop length increases. This is shown by a dispersion plot (see Figure 4.1). Since the wave frequency is a measure of the number of oscillations over length in a given time, you would expect this value to decrease as the wave has an increasing distance over which to travel.

4.1.2 Numerical results

We can plot dispersion diagrams for different values of h, the extent of the chromospheric footpoints. Figure 4.2 shows the first wave four wave modes for small h ($h = 10$ m and $h = 1000$ m=1 km), whilst we can use Figure 4.3 to compare the first four wave modes for larger values of h ($h = 10^3$ km and $h = 10^4$ km).

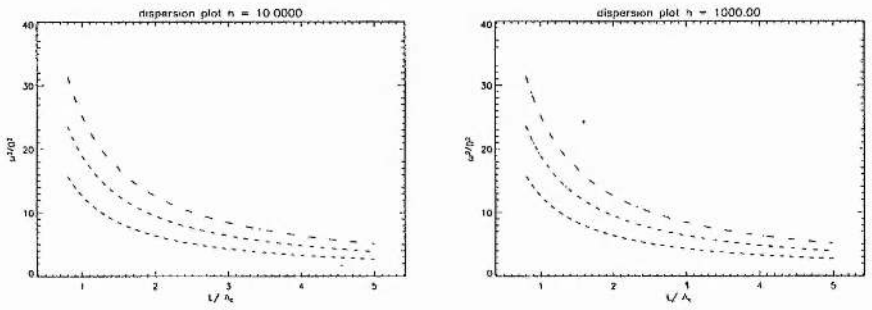

(a) Dispersion plot for $h = 10$ m. (b) Dispersion plot for $h = 1000$ m.

Figure 4.2: Dispersion diagram showing how the dimensionless frequency $\overline{\omega} = \omega/\Omega_c$ changes with varying $s = L/\Lambda_c$, for small h.

Using

$$\Omega_c^2 = \frac{1}{4}\frac{\gamma^2 g^2}{c_c^2} = 2 \times 10^{-6}\mathrm{s}^{-2},$$

we can find the period

$$\tau = \frac{2\pi}{\omega} = \frac{2\pi}{\overline{\omega}\,\Omega_c}.$$

Using the numerical code, values for $\overline{\omega}$ can be found for varying L, and we can calculate the percentage change of the period when the chromosphere is included in the model. Table 4.2 compares the dimensionless frequency $\overline{\omega}$ and period τ found for the minimum and maximum loop lengths for the full model

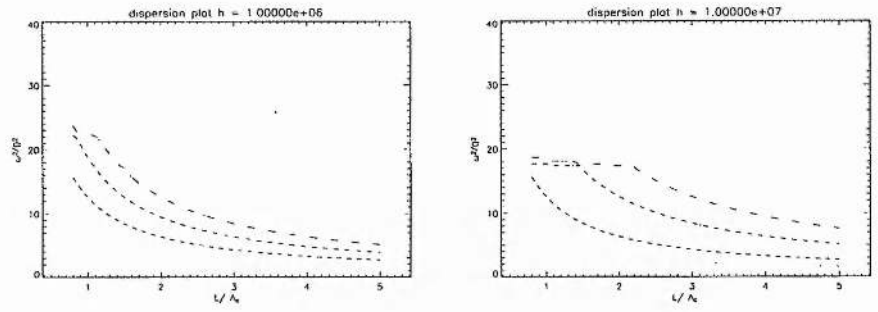

(a) Dispersion plot for $h = 10^3$ km. (b) Dispersion plot for $h = 10^4$ km.

Figure 4.3: Dispersion diagram showing how the dimensionless frequency $\overline{\omega} = \omega/\Omega_c$ changes with varying $s = L/\Lambda_c$, for large h.

and for the isolated slab. It shows how the effect of the chromosphere lessens as the loop length increases, by calculation of the percentage change of the period when incrementing h in steps from 50 Mm to 200 Mm. The change in period is slight, which seems a little surprising. One would expect the increased density in the chromosphere to have a greater impact. The chromosphere does have more impact for shorter loop lengths, which is expected.

Considering an average loop of length $L = 110$ Mm we can calculate the value of the wavenumbers $k_{c,p}$. Since the value of h does not appear to affect the model, it does not matter what value we use. We calculate $\overline{\omega}$ for several values of h and obtain a value $\overline{\omega}$ correct to 2 decimal places,

$$\overline{\omega} = 3.02.$$

From this value we can calculate $k_{c,p}$, through

$$k_c^2 = \frac{\Omega_c^2(\overline{\omega}^2 - 1)}{c_c^2}, \quad k_p^2 = \frac{\Omega_c^2\overline{\omega}^2 - \Omega_p^2}{c_p^2}. \tag{4.4}$$

These equations provide us with values of $k_c^2 = 1.7486 \times 10^{-10}$ km^{-2}, $k_p^2 = -8.6 \times 10^{-7}$ km^{-2}. This shows us that the wave in the chromospheric layer is evanescent, since k_p will be imaginary.

From this analysis we can conclude that the chromospheric layer does effect the wave propagation, showing that the wave is evanescent in this layer. However, the impact of the chromosphere compared to the large coronal layer is minimal, and it is only noticeable for shorter loops, of half-length < 100 Mm.

Half-length of Loop (Mm)	No Chromosphere	Chromosphere	% change
L_{min}=40	$\overline{\omega} = 7.917$	$\overline{\omega} = 7.883$	
	$\tau = 561.2$s	$\tau = 563.6$s	0.5
$L = 50$	$\overline{\omega} = 6.362$	$\overline{\omega} = 6.330$	
	$\tau = 698.4$s	$\tau = 701.9$s	0.5
$L = 75$	$\overline{\omega} = 4.307$	$\overline{\omega} = 4.297$	
	$\tau = 1031.6$s	$\tau = 1034.0$s	0.3
$L = 100$	$\overline{\omega} = 3.297$	$\overline{\omega} = 3.292$	
	$\tau = 1347.6$s	$\tau = 1349.6$s	0.15
$L = 125$	$\overline{\omega} = 2.705$	$\overline{\omega} = 2.701$	
	$\tau = 1642.5$s	$\tau = 1644.9$s	0.15
$L = 150$	$\overline{\omega} = 2.321$	$\overline{\omega} = 2.319$	
	$\tau = 1914.2$s	$\tau = 1915.9$s	0.1
$L = 175$	$\overline{\omega} = 2.055$	$\overline{\omega} = 2.053$	
	$\tau = 2162.0$s	$\tau = 2164.1$s	0.1
$L = 200$	$\overline{\omega} = 1.862$	$\overline{\omega} = 1.861$	
	$\tau = 2386.1$s	$\tau = 2387.4$s	0.05
$L = 225$	$\overline{\omega} = 1.717$	$\overline{\omega} = 1.716$	
	$\tau = 2587.6$s	$\tau = 2589.1$s	0.05
$L_{max} = 245$	$\overline{\omega} = 1.626$	$\overline{\omega} = 1.625$	
	$\tau = 2732.4$s	$\tau = 2734.1$s	0.05

Table 4.2: Effect of the chromosphere on the period τ, comparing values obtained for $h = 0$ and $h = 10^7$m.

4.2 Effect of gravity

Aside from the chromospheric footpoints, it is important to look at the impact of gravity on this model. In section 3.2.2 we found the governing differential equation for wave propagation in isothermal medium of extent L:

$$\frac{d^2Q}{dz^2} + k^2Q = 0. \tag{4.5}$$

On applying zero velocity at the loop ends to the solution

$$Q = A\cos k_c z + B\sin k_c z, \tag{4.6}$$

where A, B are constants, we obtained the dispersion relation (equation 3.20)

$$\omega^2 = \frac{n^2\pi^2 c_c^2}{L^2} + \Omega_c^2, \tag{4.7}$$

where

$$\Omega_c^2 = \frac{1}{4}\frac{\gamma^2 g^2}{c_c^2}, \quad c_c^2 = \text{constant}. \tag{4.8}$$

We investigate the effect of gravity on the period τ,

$$\tau = \frac{2\pi}{\omega} = \frac{2\pi}{\left(\frac{n^2\pi^2 c_c^2}{L^2} + \Omega_c^2\right)^{1/2}}. \tag{4.9}$$

When $g = 0$ this simplifies (since $\Omega_c^2 = 0$) to

$$\tau = \frac{2L}{nc_c}. \tag{4.10}$$

When $g \neq 0$, we have

$$\begin{aligned}
\tau &= 2\pi\left[\frac{n^2\pi^2 c_c^2}{L^2} + \frac{1}{4}\frac{\gamma^2 g^2}{c_c^2}\right]^{-1/2} \\
&= 2\pi\frac{L}{n\pi c_c}\left[1 + \frac{1}{4}\frac{\gamma^2 g^2}{c_c^2}\frac{L^2}{n^2\pi^2 c_c^2}\right]^{-1/2} \\
&= \frac{2L}{nc_c}\left[1 + \frac{1}{4}\frac{c_4^2}{\Lambda_c^2 c_c^2}\frac{L^2}{n^2\pi^2 c_c^2}\right]^{-1/2}, \quad c_c^2 = \gamma g \Lambda_c \\
&= \frac{2L}{nc_c}\left[1 + \frac{L^2}{4n^2\pi^2\Lambda_c^2}\right]^{-1/2}.
\end{aligned} \tag{4.11}$$

Assuming that $L \ll \Lambda_c$ (or more specifically that $L \ll 2n\pi\Lambda_c$), the bracketed term can be expanded, using a Binomial series, to give

$$\tau = \frac{2L}{nc_c}\left[1 - \frac{L^2}{8n^2\pi^2\Lambda_c^2}\right]. \tag{4.12}$$

A similar result is found if slightly different boundary conditions to the differential equation (4.5) are used. For example, allowing for wave leakage at the footpoints by taking

$$\frac{dQ}{dz} = 0 \text{ at } z = L, \tag{4.13}$$

in place of $Q = 0$ at $z = L$, the results given in section 3.1 change only slightly. Imposing $Q = 0$ at $z = 0$ reduced Q to

$$Q = B\sin k_c z. \tag{4.14}$$

Introducing the new boundary condition (4.13) gives

$$\cos k_c z = 0, \quad k_c L = \left(n + \frac{1}{2}\right)\pi, \quad n = 0, 1, 2, ... \tag{4.15}$$

i.e. we have replaced n by $n + 1/2$. Thus, the period τ (equation (4.12)) is given by

$$\tau = \frac{2L}{\left(n + \frac{1}{2}\right) c_c}\left[1 - \frac{L^2}{8\left(n + \frac{1}{2}\right)^2 \pi^2 \Lambda_c^2}\right]. \tag{4.16}$$

The period τ has a correction determined by

$$\Delta\tau_{gravity} = \frac{L^2}{8\left(n + \frac{1}{2}\right)^2 \pi^2 \Lambda_c^2}. \tag{4.17}$$

Consequently, this correction will be negligible if

$$L^2 \ll 8\left(n + \frac{1}{2}\right)^2 \pi^2 \Lambda_c^2,$$

i.e. if n is large or the coronal loop is short. Since L corresponds to the half-length of a coronal loop, we write $L = \lambda \times 10^8$m. Taking the first wave mode $n = 1$, the expression for the effect of gravity, $\Delta\tau_{gravity}$, can be simplified. Using a coronal pressure scale height $\Lambda_c = 5 \times 10^7$m, we obtain

$$\Delta\tau_{gravity} = 0.0028\lambda^2. \tag{4.18}$$

This immediately shows you that for an average half-loop length $L = L_{ave} = 110$ Mm, $\Delta\tau_{gravity} = 3\%$ and for a longer half-loop length $L = L_{max} = 203$ Mm, $\Delta\tau_{gravity} = 10\%$. This shows that gravity appears to have a significant impact on wave propagation, especially on longer loops.

Previously an assumption was made that the effect of gravity on the wave period was small. However, this does not appear to hold for long loops. Using the form of the period determined before this assumption was made (equation 4.11), we can analyse the effect of gravity by comparing calculated values of the period for models with and without gravity. Ofman and Aschwanden (2002) studied damping mechanisms of loop oscillations. They studied 11 oscillations for which the oscillation period and decay time could both be determined reasonably accurately. We consider the same 11 loops. The results of this analysis is shown in Table 4.3.

Loop	Date	Length (Mm)	half-length (Mm)	Period τ (secs) $g = 0$	Period τ (secs) $g \neq 0$	$\Delta\tau_{gravity}$
1	1998 Jul 14	168	84	1120000	1081990	3.5 %
2	1998 Jul 14	72	36	480000	476879	0.7 %
3	1998 Jul 14	174	87	1160000	1117925	3.8 %
4	1998 Jul 14	204	102	1360000	1293530	5.1 %
5	1998 Jul 14	162	81	1080000	1045799	3.3 %
6	1998 Nov 23	390	195	2600000	2209050	17.7 %
7	1999 Jul 04	258	129	1720000	1591087	8.1 %
8	1999 Oct 25	166	83	1106666	1069955	3.4 %
9	2001 Mar 21	406	203	2706666	2273359	19.1 %
10	2001 May 15	192	97	1280000	1224123	4.6 %
11	2001 Jun 15	146	73	973333	948075	2.7 %

Table 4.3: The percentage change $\Delta\tau_{gravity}$ of the period for a gravity model compared to a non-gravity model. The data for the 11 loops comes from Aschwanden and Ofman (2002).

Table 4.3 shows what appears to be a definite link between the effect of gravity, ie the percentage change of the period, and the length of the loop. For the smallest loop, the change is less than 1%; however, this rises to almost 20% for the largest loop of total length 406 Mm. This relationship is illustrated in Figure 4.4.

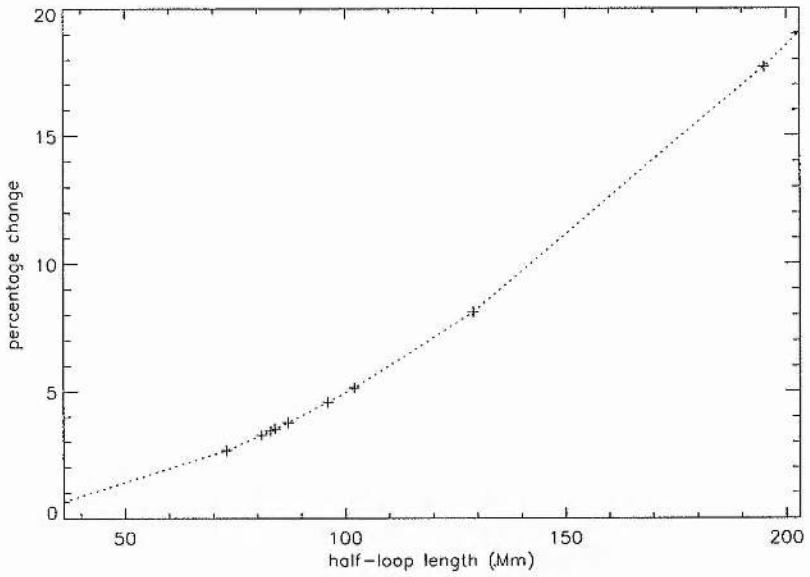

Figure 4.4: Plot showing how the loop length affects the change that gravity has on the period of acoustic oscillations. The crosses mark the 11 datapoints discussed by Aschwanden and Ofman (2002) and the dotted line is extrapolated between them.

4.3 Applying theory to SUMER data

As outlined in section 1.6, several papers have been written recently on the observations of damped oscillations of hot coronal loops in Doppler shift seen by the Solar Ultraviolet Measurements of Emitted Radiation (SUMER) on SOHO. These observations show oscillations which have periods in the range $P = 7-31$ minutes and average decay times of $\tau_d = 6.37$ minutes. Wang *et al.* (2003) reported on observational evidence that these Doppler shifts are the result of slow-mode standing waves in high temperature loops. They use a result from Roberts, Edwin and Benz (1984) that slow-mode standing waves in a loop of

length $\mathcal{L}$ have a period P given by

$$P_{slow} = \frac{2\mathcal{L}}{c_s}. \tag{4.19}$$

There are two examples in the literature of hot temperature loop oscillations where both the observed period and the corresponding loop length are described. Both of these cases give suitable values of the period P_{slow} (see Table 4.4) when using a sound speed of 382 kms^{-1}, corresponding to a temperature of 6.3 MK.

Loop	Loop length (Mm)	P_{obs} (min)	P_{slow} (min)
1	140	14-18	12.22
2	191	17.6 $\pm$ 0.1	16.7

Table 4.4: Comparison of observed period, P_{obs} and the period P_{slow}, calculated for the slow mode using equation (4.19), for data from Loop 1. Wang *et al.* (2002a) and Loop 2. Wang *et al.* (2003).

This alone does not show that the waves are slow modes. There are two other wave modes - fast and kink - which need to be considered. The fast sausage mode can quickly be rejected, for in thin flux tubes, such as hot-temperature loops, only slow and kink modes propagate (Roberts, Edwin and Benz 1984). There are two arguments that can be considered for the kink mode. The first uses another formula from Roberts, Edwin and Benz (1984), this time for the period, P_{kink}, of a kink mode,

$$P_{kink} = \frac{2\mathcal{L}}{c_k}, \qquad c_k = c_A \left(\frac{2}{1 + n_e/n_0} \right)^{1/2}, \tag{4.20}$$

where $n_{e,0}$ is the electron density outside and inside the loop respectively, and $c_A = 2.18 \times 10^{11} B n_0^{-1/2} \approx 1100$ kms^{-1}is the Alfvén speed inside the loop. Assuming $n_e/n_0 \sim 0.1$, the period obtained is approximately 4 times smaller than observed (see Table 4.5). For the period of the kink mode to match the observed period, the plasma beta β $[=(2/\gamma)(c_s^2/c_A^2)]$ would have to be ≈ 2. However this implies a density 25 times greater or a magnetic field 5 times weaker (Wang *et al.* 2002a).

Another compelling reason to reject the kink mode emerges when one considers the displacement amplitude of the loop oscillations. Given a velocity amplitude of 100 kms^{-1}and the observed periods of approximately 20 minutes we would expect loop displacements of about 20,000 km. This scale is theo-

Loop	Loop length (Mm)	P_{obs} (min)	P_{kink} (min)
1	140	14-18	3.15
2	191	17.6 ± 0.1	4.29

Table 4.5: Comparison of observed period, P_{obs}, and the period P_{kink}, calculated for the kink mode using (4.20), for data from Loop 1. Wang *et al.* (2002a) and Loop 2. Wang *et al.* (2003)

retically observable by the Soft X-ray instrument on SUMER; however, such displacements are not observed. In fact, such lack of observations lends weight to the argument that the oscillations are slow mode waves, for slow modes do not significantly displace the loop.

We now consider whether these waves are standing or propagating waves. We can do this by studying the phase difference between velocity and intensity, for propagating waves give an in-phase variation whereas standing waves give a 1/4-period phase difference (Sakurai *et al.* 2002).

From the assumption that these waves are a slow standing mode, we can analyse the form of the wave and calculate the phase difference between velocity and intensity, $\delta I/I$. Consider a wave with velocity of the form

$$v(x,t) = V\cos(kz)\cos(kc_s t)\exp(-\lambda t), \tag{4.21}$$

where the magnetic field of the loop is taken to be along the z-direction, V is the amplitude and k is the wavenumber. Wang *et al.* (2003) studied this wave form using the linearised continuity equation for a perturbed density $\rho = \rho_0 + \rho_1$, $\rho_1 \ll \rho_0$,

$$\frac{\partial \rho_1}{\partial t} + \mathrm{div}(\rho_0 \mathbf{v}) = 0. \tag{4.22}$$

Wang *et al.* al assumed a constant background density ρ_0. However, we can apply the gravity model developed in here, with a density profile given by

$$\rho_0' = \frac{d\rho_0}{dz} = \rho_0 g, \tag{4.23}$$

where $'$ denotes the derivative with respect to z. This means that the linearised continuity equation has an extra term for

$$\mathrm{div}(\rho_0 \mathbf{v}) = \rho_0 \frac{\partial v}{\partial z} + \rho_0' v. \tag{4.24}$$

Taking v_z of the form of equation (4.21), the linearised continuity equation becomes

$$\frac{\partial \rho_1}{\partial t} = -kV_0\rho_0 \cos(kz)\cos(\omega t) - V_0\rho_0' \sin(kz)\cos(\omega t).$$

Thus, we may take

$$\rho_1 = -\frac{kV_0}{\omega}\rho_0 \cos(kz)\sin(\omega t) - \frac{V_0}{\omega}\rho_0' \sin(kz)\sin(\omega t). \tag{4.25}$$

To continue this analysis we need to find an expression for ρ_0'. With $\mathbf{g} = g\mathbf{e}_z$, so that gravity is aligned with the z-axis, the perfect gas law (2.6) provides a relationship between p_0 and ρ_0,

$$\rho_0 = \frac{p_0 m}{k_B T_0}. \tag{4.26}$$

An expression for p_0 was found in section 2.9, namely,

$$p_0(z) = p_0(0)\ \exp n(z), \qquad n(z) = \int_0^z \frac{dz}{\Lambda_c},$$

where Λ_c is the scale height.

Using this information an expression for ρ_0 and ρ_0' is obtained,

$$\rho_0 = \rho_0(0)e^{z/\Lambda_c}, \quad \rho_0' = \frac{\rho_0(0)}{\Lambda_c}e^{z/\Lambda_c} \tag{4.27}$$

Wang *et al.* (2003) form the fraction $\delta I/I$; following their example and using (4.25) and (4.27), we obtain:

$$\begin{aligned}\frac{\delta I}{I} = \frac{2\rho_1}{\rho_0} &= -\frac{2V_0}{\omega}\left[k\cos(kz) + \frac{1}{\Lambda_c}\frac{\rho_0(0)e^{z/\Lambda_c}}{\rho_0(0)e^{z/\Lambda_c}}\sin(kz)\right]\sin(\omega t) \\ &= -\frac{2V_0}{\omega}\sin(\omega t)\left[k\cos(kz) + \frac{1}{\Lambda_c}\sin(kz)\right]\end{aligned} \tag{4.28}$$

Now $\sin(\omega t)$ is at most 1, so equation (4.28) implies that

$$\left|\frac{\delta I}{I}\right| \leq \left|\frac{2V_0}{\omega}\left[k\cos(kz) + \frac{1}{\Lambda_c}\sin(kz)\right]\right|.$$

Thus, for k positive, $\delta I/I$ reduces to

$$\left|\frac{\delta I}{I}\right| \leq \frac{2V_0}{\omega}\left[k + \frac{1}{\Lambda_c}|\tan(kz)|\right]. \tag{4.29}$$

Using values from Wang *et al.* (2003): $\delta I/I = 0.19$, $k = \pi/L$, $c_s = 380$ kms^{-1}, $L = 191$ Mm, $V_z = 18.6$ kms^{-1}, we can then form the combinations:

$$\frac{k^2 c_s^2}{\omega^2} = 190, \quad \omega^2 = \frac{\pi^2/L^2 \times 380^2}{190} = \frac{760\pi^2}{L^2}, \quad \omega = \frac{27.568\pi}{L}$$

$$\Lambda_c = \frac{c_s^2}{\gamma g} = \frac{380^2}{\frac{5}{3} \times 0.274} = 320889\text{km}$$

Substituting these values into (4.29) gives us the estimate

$$|\tan(kz)| = 1.9166. \tag{4.30}$$

This gives a value of 1.08989 for kz, which in turn produces a value of $0.347L$ for z. Wang *et al.* (2003) found a value of 1.94 for $|\tan(kz)|$ and a value of $0.35L$ for z.

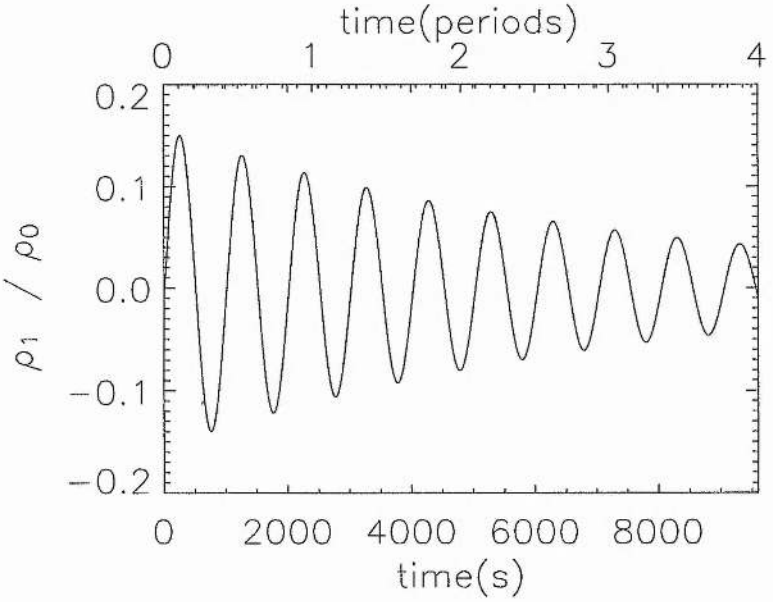

Figure 4.5: Plot ρ_1/ρ_0 evolves in time.

This analysis shows that the gravity model can be applied to other situations, such as the slow standing waves observed by SUMER. The shape of the waves can be seen by plotting ρ_1/ρ_0 and examining the time variation, as shown in Figure 4.5.

Chapter 5

Conclusion

5.1 Thesis summary

The observed damping of wave oscillations in coronal loops is important and may be due to many factors. In order to consider this we have looked at a number of areas.

Chapter 1 gave an introduction to the Sun and the way observations from satellites such as TRACE and SUMER have stimulated many papers on oscillations in coronal loops. We discussed the impact of the Nakariakov *et al.* (1999) paper that was the first to analyse strong damping of TRACE loop oscillations. Since then many papers have been written and theories produced on why the oscillations are observed to have such strong damping. Theories of wave leakage at the footpoints, resonant absorption and phase mixing have been discussed by Roberts (2000), Ruderman and Roberts (2002), Aschwanden and Ofman (2002) and De Pontieu *et al.* (2001), among others.

Chapter 2 outlined the MHD equations and how we can use these to study wave phenomena through the process of linearisation. We outlined the many wave forms discussed in the literature and showed in detail how the MHD equations can be used to consider waves in a uniform medium, waves at a magnetic interface, and waves in a magnetic slab. At the end of the chapter, in order to lead into the analysis of Chapter 3, details were given of the description of acoustic waves in an atmosphere with gravity.

Chapter 3 built up our coronal loop model. We considered two ways of describing the gravity stratification and the impact of a chromospheric layer, either by having two media separated at a discontinuous interface (section 3.2), or having a continuously varying sound speed (section 3.3). It was concluded in this chapter that the discontinuous interface was the more robust of the two and this analysis we used for our results in Chapter 4.

5.2 The impact of a chromospheric layer

By using a numerical code based upon the bisection method, we found roots of the dispersion relation for a two-layer isothermal atmosphere. On comparison with roots for a single isothermal atmosphere it was found that the embedding of footpoints in a chromospheric layer below the corona made little impact on the periods of waves travelling through the medium. The greatest effect was for shorter loops, where the percentage change of the period was 0.5%. This is perhaps not a surprising result for even considering the deepest chromospheric layer (put forward by various authors) of 10^7m, this depth is only four percent of the length of the largest observed coronal loops that support damping oscillations.

5.3 The impact of gravity

The period of wave oscillations in our model showed a definite change when stratification due to gravity was added. Although the effect was small for short loops, of half-length 5×10^7m, the percentage change in the period rose from 1% to almost 20% for the loops of half-length 200 Mm. Thus this effect is important for the modelling of coronal loop oscillations in long loops.

5.4 Possible future work

Since gravity is often ignored by authors discussing loop oscillations, more work needs to be done considering the coupling of gravity and magnetic field and to see what impact gravity will have in a magnetohydrodynamic model. The Bessel results obtained when considering a single medium with a sound speed that varies along the loop can be further investigated. Such discussions are likely to be complicated, but it is to be expected that results obtained here for acoustic waves will be relevant also for slow modes in a coronal loop.

The application of this model to data can continue, for the comparison of this model with SUMER data shows that it can be applied to real observations.

Appendix A

Boundary Condition

To find an interface boundary condition for the solution (3.10), of the differential equation (3.7) obtained in section 3.2 consider the differential equation

$$\frac{d^2Q}{dz^2} = -\frac{\omega^2}{c_s^2(z)}Q(z) + \frac{\Omega^2(z)}{c_s^2(z)}Q(z).$$

Integrate over a small neighbourhood of $z = L$, namely from $z = L - \epsilon$ to $z = L + \epsilon$, where ϵ is small,

$$\int_{L-\epsilon}^{L+\epsilon} \frac{d^2Q}{dz^2}dz = -\int_{L-\epsilon}^{L+\epsilon} \frac{\omega^2}{c_s^2(z)}Q(z)\,dz + \int_{L-\epsilon}^{L+\epsilon} \frac{\Omega^2(z)}{c_s^2(z)}Q(z)\,dz. \tag{A.1}$$

The left-hand side of equation (A.1) simplifies as follows,

$$\int_{L-\epsilon}^{L+\epsilon} \frac{d^2Q}{dz^2}dz = \frac{dQ}{dz}\bigg|_{L-\epsilon}^{L+\epsilon} = \frac{dQ}{dz}\bigg|_{L+\epsilon} - \frac{dQ}{dz}\bigg|_{L-\epsilon}. \tag{A.2}$$

Considering the first term on the right-hand side of equation (A.1), since $\omega^2 Q(z)$ is continuous and $c_s^2(z)$ is at most a step function, the integral will tend to zero as ϵ tends to zero, i.e.

$$\int_{L-\epsilon}^{L+\epsilon} \frac{\omega^2}{c_s^2(z)}Q(z)\,dz \to 0 \text{ as } \epsilon \to 0. \tag{A.3}$$

Considering the second term on the right-hand side of equation (A.1), it can be expanded using the definition of Ω^2 (equation (2.72)):

$$\int_{L-\epsilon}^{L+\epsilon} \frac{\Omega^2(z)}{c_s^2(z)}Q(z)\,dz = \frac{1}{4}\int_{L-\epsilon}^{L+\epsilon} \frac{\gamma^2 g^2}{c_s^2}\cdot\frac{1}{c_s^2}Q\,dz - \frac{1}{2}\gamma g\int_{L-\epsilon}^{L+\epsilon} \frac{(c_s^2)'}{c_s^4}Q\,dz, \tag{A.4}$$

where a dash (') denotes differentiation with respect to z.

The first term of on right of expression (A.4) tends to zero as ϵ tends to zero for the same reason that lead to (A.3). Considering the second term, it is useful to introduce the pressure scale height,

$$\Lambda = \frac{c_s^2}{\gamma g}. \tag{A.5}$$

Then the second term on the right-hand side of equation (A.1) may be rewritten

$$\begin{aligned}\frac{1}{2}\gamma g \int_{L-\epsilon}^{L+\epsilon} \frac{(c_s^2)'}{c_s^4} Q \, dz &= \frac{1}{2}\gamma g \int_{L-\epsilon}^{L+\epsilon} \frac{\gamma g \Lambda'}{\gamma^2 g^2 \Lambda^2} Q \, dz \\ &= -\frac{1}{2}\int_{L-\epsilon}^{L+\epsilon} \frac{d}{dz}\left(\frac{-1}{\Lambda}\right) Q \, dz \end{aligned} \tag{A.6}$$

Since $c_s^2(z)$ is at most a step function, $\Lambda(z)$ is at most a step function. Then Λ' is at most a delta function. Using this fact we can take the value of Q at $z = L$ out of the integral,

$$\begin{aligned}\frac{1}{2}\gamma g \int_{L-\epsilon}^{L+\epsilon} \frac{(c_s^2)'}{c_s^4} Q \, dz &= -\frac{Q(L)}{2}\int_{L-\epsilon}^{L+\epsilon} \frac{d}{dz}\left(\frac{-1}{\Lambda}\right) dz \\ &= \frac{1}{2} Q(L) \left.\frac{1}{\Lambda}\right|_{L-\epsilon}^{L+\epsilon}. \end{aligned} \tag{A.7}$$

Combining the results (A.2), (A.3) and (A.7) gives

$$\frac{dQ}{dz} = \frac{Q}{2\Lambda}, \qquad \text{evaluated at } z = L.$$

Thus,

$$\frac{dQ}{dz} - \frac{1}{2\Lambda_0} Q \text{ is continuous at } z = L. \tag{A.8}$$

The same condition can be found by considering the original variables ρ_0, p_1 and v_z using the relating equation

$$-\omega^2 \rho_0 v_z + i\omega \frac{dp_1}{dz} + g\frac{d}{dz}(\rho_0 v_z) = 0. \tag{A.9}$$

Integrating expression (A.9) over a small neighbourhood of $z = L$ gives

$$i\omega p_1 + g\rho_0 v_z \text{ is continuous at } z = L,$$

which is equivalent to

$$-c_s^2 \rho_0 \frac{dv_z}{dz} \text{ is continuous at the interface.} \tag{A.10}$$

Converting expression (A.10) to the variable Q, the boundary condition equation (A.8) is obtained.

Appendix B

Dimensionless Dispersion Relation

To obtain a dimensionless dispersion relation in terms of the dimensionless frequency $\overline{\omega} = \omega/\Omega_c$ (equation (3.37)), we must write $k_c L$, $k_p h$, $k_c \Lambda_c$ and $k_p \Lambda_c$ in terms of $\overline{\omega}$. To do so we must use the definitions

$$k_{c,p}^2 = \frac{\omega^2 - \Omega_{c,p}^2}{c_{c,p}^2}, \quad \text{and} \quad \Omega_{c,p}^2 = \frac{1}{4}\frac{\omega^2 g^2}{c_{c,p}^2} = \frac{1}{4}\frac{c_{c,p}^2}{\Lambda_{c,}^2} \tag{B.1}$$

It is useful to introduce the following dimensionless variables,

$$r = \frac{\Lambda_p}{\Lambda_c} = \frac{c_p^2}{c_c^2} \quad s = \frac{L}{\Lambda_c}, \quad \text{and} \quad \zeta = \frac{h}{\Lambda_c}. \tag{B.2}$$

The four terms involving $k_{c,p}$ then expand as follows:

$$\begin{aligned} k_c^2 L^2 = \left(\frac{\omega^2 - \Omega_c^2}{c_c^2}\right) L^2 &= \frac{\omega^2 L^2}{c_c^2} - \frac{\Omega_c^2 L^2}{c_c^2} \\ &= \Omega_c^2 \frac{L^2}{c_c^2}\left(\frac{\omega^2}{\Omega_c^2} - 1\right) \\ &= \frac{L^2}{c_c^2}\frac{1}{4}\frac{c_c^2}{\Lambda_c^2}\left(\overline{\omega}^2 - 1\right) \\ &= \frac{s^2}{4}\left(\overline{\omega}^2 - 1\right) \end{aligned} \tag{B.3}$$

$$k_p^2 h^2 = \left(\frac{\omega^2 - \Omega_p^2}{c_p^2}\right) h^2 = \frac{\omega^2}{\Omega_c^2}\,\frac{\Omega_c^2 h^2}{c_p^2} - \frac{\Omega_p^2 h^2}{c_p^2}$$
$$= \overline{\omega}^2\,\frac{1}{4}\,\frac{c_c^2}{\Lambda_c^2}\,\frac{h^2}{c_p^2} - \frac{1}{4}\,\frac{c_p^2}{\Lambda_p^2}\,\frac{h^2}{c_p^2}$$
$$= \frac{\zeta^2}{4r}\left(\overline{\omega}^2 - \frac{1}{r}\right) \tag{B.4}$$

$$k_c^2 \Lambda_c^2 = \left(\frac{\omega^2 - \Omega_c^2}{c_c^2}\right) \Lambda_c^2 = \frac{\Omega_c^2 \Lambda_c^2}{c_c^2}\left(\frac{\omega^2}{\Omega_c^2} - 1\right)$$
$$= \frac{1}{4}\,\frac{c_c^2}{\Lambda_c^2}\,\frac{\Lambda_c^2}{c_c^2}\left(\overline{\omega}^2 - 1\right)$$
$$= \frac{1}{4}\left(\overline{\omega}^2 - 1\right) \tag{B.5}$$

$$k_p^2 \Lambda_c^2 = \left(\frac{\omega^2 - \Omega_p^2}{c_p^2}\right) \Lambda_c^2 = \frac{\omega^2}{\Omega_c^2}\,\frac{\Lambda_c^2 \Omega_c^2}{c_p^2} - \frac{\Omega_p^2 \Lambda_c^2}{c_p^2}$$
$$= \overline{\omega}^2\,\frac{\Lambda_c^2}{c_p^2}\,\frac{1}{4}\,\frac{c_c^2}{\Lambda_c^2} - \frac{\Lambda_c^2}{c_p^2}\,\frac{1}{4}\,\frac{c_p^2}{\Lambda_p^2}$$
$$= \frac{1}{4r}\left(\overline{\omega}^2 - \frac{1}{r}\right) \tag{B.6}$$

Appendix C

Solar Values

$$\text{Adiabatic constant} \qquad \gamma = \frac{5}{3}. \tag{C.1}$$

$$\text{Gravity} \qquad g = 0.274 \text{ km s}^{-1}. \tag{C.2}$$

$$\text{Sound speed} \qquad c = 152\, T^{1/2} \text{ m s}^{-1}, \tag{C.3}$$

where T is the temperature in Kelvin.

$$\text{Pressure scale height} \qquad \Lambda = \frac{c^2}{\gamma g}. \tag{C.4}$$

The above equations can give values for c_c, c_p, Λ_c and Λ_p on using suitable temperature values. For the corona a valid temperature is $T = 10^6$K and for the chromospheric/photospheric layer a valid temperature is $T = 10^4$K.

$$\begin{aligned} c_c &= 152 \times (10^6)^{1/2} \text{ m s}^{-1}, \\ &= 152000 \text{ m s}^{-1}, \\ &\approx 152 \text{ km s}^{-1}. \end{aligned} \qquad \begin{aligned} c_p &= 152 \times (10^4)^{1/2} \text{ m s}^{-1}, \\ &= 15200 \text{ m s}^{-1}, \\ &\approx 15 \text{ km s}^{-1}. \end{aligned} \tag{C.5}$$

(C.6)

$$\begin{aligned} \Lambda_c &= \frac{150^2}{\frac{5}{3} \times 0.274} \text{ km}, \\ &= 49270 \text{ km}, \\ &\approx 5 \times 10^4 \text{ km}. \end{aligned} \qquad \begin{aligned} \Lambda_p &= \frac{15^2}{\frac{5}{3} \times 0.274} \text{ km}, \\ &= 492.7 \text{ km}, \\ &\approx 500 \text{ km}. \end{aligned} \tag{C.7}$$

A useful value to find is $\Omega_{c,p}^2$,

$$\Omega_{c,p}^2 = \frac{1}{4}\,\frac{\gamma^2 g^2}{c_{c,p}^2}.$$

$$\begin{aligned}
\Omega_c^2 &= \frac{1}{4}\,\frac{\frac{5^2}{3^2}\,0.274^2(\mathrm{km\ s^{-1}})^2}{152^2(\mathrm{km})^2}, & \Omega_p^2 &= \frac{1}{4}\,\frac{\frac{5^2}{3^2}\,0.274^2(\mathrm{km\ s^{-1}})^2}{15^2(\mathrm{km})^2}, \\
&= 0.0000023\ \mathrm{s^{-2}}, & &= 0.00023\ \mathrm{s^{-2}}, \\
&\approx 2\times 10^{-6}\ \mathrm{s^{-2}} & &\approx 2\times 10^{-4}\ \mathrm{s^{-2}}. \qquad \text{(C.8)}
\end{aligned}$$

Appendix D

Zeros of Cross-Products of Bessel Functions

Abramowitz and Stegun (1964) state the result that

$$\mathcal{J}_\nu(z)\mathcal{Y}_\nu(\lambda z) - \mathcal{Y}_\nu(z)\mathcal{J}_\nu(\lambda z) = 0 \tag{D.1}$$

has asymptotic solutions if $\lambda > 1$.

The asymptotic expansion of the sth root is

$$z = \beta + \frac{p}{\beta} + \frac{q - p^2}{\beta^3} + \frac{r - 4pq + 2p^3}{\beta^5} + \ldots \tag{D.2}$$

where, with $4\nu^2$ denoted by μ,

$$\beta = \frac{s\pi}{\lambda - 1}, \tag{D.3}$$

$$p = \frac{\mu - 1}{8\lambda}, \tag{D.4}$$

$$q = \frac{(\mu - 1)(\mu - 25)(\lambda^3 - 1)}{6(4\lambda)^3(\lambda - 1)}, \tag{D.5}$$

$$r = \frac{(\mu - 1)(\mu^2 - 114\mu + 1073)(\lambda^5 - 1)}{5(4\lambda)^5(\lambda - 1)}. \tag{D.6}$$

The dispersion relation we have of this form, found for the sound speed of the form $c_s(z) = c_0(1 - \alpha z)^{1/2})$, is

$$\mathcal{J}_\nu\left(\frac{2\omega}{\alpha c_o}\right)\mathcal{Y}_\nu\left(\frac{2\omega}{\alpha c_o}\frac{c_{base}}{c_0}\right) - \mathcal{J}_\nu\left(\frac{2\omega}{\alpha c_o}\frac{c_{base}}{c_0}\right)\mathcal{Y}_\nu\left(\frac{2\omega}{\alpha c_o}\right) = 0. \tag{D.7}$$

(Equation 3.68 in section 3.3.2).

Taking typical sound speeds $c_0 = 150$, $c_{base} = 15$ gives

$$\frac{c_{base}^2}{c_0^2} = 1 - \alpha(L+h),$$

$$\alpha \times 10^5\text{km} = 1 - \frac{15^2}{150^2},$$

$$\alpha = \frac{99}{100}10^{-5}\text{km}^{-1} \approx 10^{-5}\text{km}^{-1}. \tag{D.8}$$

This means we can work through the other variables ν, μ, λ, β, p, q and r and calculate values for them.

$$\nu = 1 + \frac{\gamma g}{\alpha c_0^2} = 1 + \frac{\frac{5}{3} \times 0.274}{10^{-5} \times 150^2} = 1 + \frac{0.456667}{0.225} = 3.03 \tag{D.9a}$$

$$\mu = 4\nu^2 = 4 \times 3.03^2 = 36.7236 \tag{D.9b}$$

$$\lambda = \frac{c_0}{c_{base}} = \frac{150}{15} = 10 \tag{D.9c}$$

$$\beta = \frac{s\pi}{9} \tag{D.9d}$$

$$p = \frac{35.7236}{80} = 0.446545 \tag{D.9e}$$

$$q = \frac{35.7236 \times 11.7236 \times 999}{6 \times 64000 \times 9} = \frac{418390}{3456000} = 0.12106 \tag{D.9f}$$

$$r = \frac{35.7236 \times -1764.8676 \times 99999}{5 \times 102400000 \times 9} = \frac{6304679372}{4608000000} = -1.3682 \tag{D.9g}$$

Using these values to calculate the terms in the asymptotic expansion (D.2):

$$\beta = \frac{s\pi}{9} \tag{D.10a}$$

$$\frac{p}{\beta} = \frac{9 \times 0.446545}{s\pi} = \frac{4.02}{s\pi} \tag{D.10b}$$

$$\frac{q-p^2}{\beta^3} = \frac{9^3 \times (0.12106 - 0.446545^2)}{s^3\pi^3} = \frac{-57.112}{s^3\pi^3} \tag{D.10c}$$

$$\frac{r - 4pq + 2p^3}{\beta^5} = \frac{9^5 \times (-1.3682 - 4 \times 0.4465 \times 0.12106 + 2 \times 0.4465^3)}{s^5\pi^5}$$

$$= \frac{-83046.78}{s^5\pi^5} \tag{D.10d}$$

Using these values we find a value for z which, using the definition of z (equation 3.70),

$$z = \frac{c_{base}}{c_0}\frac{2\omega}{\alpha c_0}, \tag{D.11}$$

we can utilise to find a value of ω,

$$\begin{aligned}\omega &= \frac{c_0}{c_{base}}\frac{\alpha c_0}{2}z \\ &= 10 \times \frac{10^{-5} \times 150}{2}z \\ &= 0.0075z. \end{aligned} \tag{D.12}$$

Bibliography

Abramowitz, M. and Stegun, I. A., editors (1964). *Handbook of Mathematical functions with formulas, graphs, and mathematical tables.* National Bureau of Standards.

Aschwanden, M. J. (1987). Theory of radio pulsations in coronal loops. *Solar Physics*, **111**:113.

Aschwanden, M. J. (2003). Review of coronal oscillations: An observer's view. In von Fay-Siebenburgen, R., Petrovay, K., Roberts, B., and Aschwanden, M. J., editors, *Turbulence, Waves and Instabilities in the Solar Plasma, NATO Advanced Research Workshops, 16-20 Sept 2002, vol. 124*, page 215.

Aschwanden, M. J., De Pontieu, B., Schrijver, C. J., and Title, A. M. (2002). Transverse oscillations in coronal loops observed with TRACE - II. measurements of geometric and physical parameters. *Solar Physics*, **206**:99.

Aschwanden, M. J., Fletcher, L., Schrijver, C. J., and Alexander, D. (1999). Coronal loop oscillations observed with the Transition Region And Coronal Explorer. *Astrophysical Journal*, **520**:880.

De Pontieu, B., Martens, P. C. H., and Hudson, H. S. (2001). Chromospheric damping of Alfvén wave. *Astrophysical Journal*, **558**:859.

Domingo, V., Fleck, B., and Poland, A. I. (1995). The SOHO mission: an overview. *Solar Physics*, **162**:1.

Edwin, P. M. and Roberts, B. (1982). Wave propagation in a magnetically structured atmosphere III: The slab in a magnetic environment. *Solar Physics*, **76**:239.

Edwin, P. M. and Roberts, B. (1983). Wave propagation in a magnetic cylinder. *Solar Physics*, **88**:179.

Erdélyi, R. (2001). Resonant MHD waves in steady flux tubes. In Ballester, J. L. and Roberts, B., editors, *INTAS Workshop on MHD waves in Astrophysical Plasmas, 69.*

Fleck, B., Domingo, V., and Poland, A. (1995). *The SOHO mission.* Kluwer Academic Publishers.

Fröhlich, C. *et al* (1995). VIRGO: Experiment for Helioseismology and Solar Irradiance Monitoring. *Solar Physics*, **162**:101.

Gabriel, A. H. *et al* (1995). Global oscillations at low frequency from the SOHO mission (GOLF). *Solar Physics*, **162**:61.

Golub, L. and Pasachoff, J. M. (2001). *Nearest star: the surprising science of our Sun.* Harvard University Press.

Goossens, M., Andries, J., and Aschwanden, M. J. (2002). Coronal loop oscillations. an interpretation in terms of resonant absorption of quasi-mode kink oscillations. *Astronomy and Astrophysics*, **394**:L39.

Handy, B. N., Deluca, E. E., McMullen, R. A., Schrijver, C. J., Tarbell, T. D., Title, A. M., and Wolfson, C. J. (1998). The Transition Region and Coronal Explorer. *Bulletin of the American Astronomical Society*, **30**:1269.

Heyvaerts, J. and Priest, E. R. (1983). Coronal heating by phase-mixed shear Alfvén waves. *Astronomy and Astrophysics*, **117**:220.

Ibañez S., M. H. and Escalona T., O. B. (1993). Propagation of hydrodynamic waves in optically thin plasmas. *Astrophysical Journal*, **415**:335.

Ionson, J. A. (1978). Resonant absorption of Alfvénic surface waves and the heating of solar coronal loops. *Astrophysical Journal*, **226**:650.

Laing, G. B. and Edwin, P. M. (1994). Dissipation of fast magnetoacoustic waves in a cold plasma. *Solar Physics*, **151**:19.

Lamb, H. (1932). *Hydrodynamics.* Cambridge University Press.

McLean, D. J. and Sheridan, K. V. (1973). A damped train of regular metre-wave pulses from the sun. *Solar Physics*, **32**:485.

Nakariakov, V. M., Ofman, L., DeLuca, E. E., Roberts, B., and Davila, J. M. (1999). TRACE observation of damped coronal loop oscillations: Implications for coronal heating. *Science*, **285**:862.

Ofman, L. (2002). Chromospheric leakage of Alfvén waves in coronal loops. *Astrophysical Journal*, **568**:135.

Ofman, L. and Aschwanden, M. J. (2002). Damping time scaling of coronal loop oscillations deduced from transition region and coronal explorer observations. *Astrophysical Journal Letters*, **576**:L153.

Ofman, L. and Wang, T. (2002). Hot coronal loop oscillations observed by SUMER: Slow magnetosonic wave damping by thermal conduction. *Astrophysical Journal Letters*, **580**:L85.

Ogawara, Y. *et al* (1991). The solar-A mission - an overview. *Solar Physics*, **136**:1.

Priest, E. R. (1982). *Solar Magnetohydrodynamics.* Kluwer Academic Publishers.

Rae, I. C. and Roberts, B. (1982). Pulse propagation in a magnetic flux tube. *Astrophysical Journal*, **256**:761.

Ridpath, I. (1997). *Oxford dictionary of astronomy.* Oxford University Press.

Roberts, B. (1981a). Wave propagation in a magnetically structured atmosphere II: Waves in a magnetic slab. *Solar Physics*, **69**:39.

Roberts, B. (1981b). Wave propogation in a magnetically structured atmosphere I: surface waves at at magnetic interface. *Solar Physics*, **69**:27.

Roberts, B. (1991). *Advances in solar system magnetohydrodynamics*, chapter 6, Magnetohydrodynamic waves in the Sun. Cambridge University Press.

Roberts, B. (2000). Waves and oscillations in the corona - (invited review). *Solar Physics*, **193**:139.

Roberts, B. (2002). Waves and oscillations in the corona: theory. In *ESA SP-506: Solar Variability: From Core to Outer Frontiers*, page 481.

Roberts, B., Edwin, P. M., and Benz, A. O. (1984). On coronal oscillations. *Astrophysical Journal*, **279**:857.

Rosenberg, H. (1970). Evidence for MHD pulsations in the solar corona. *Astronomy and Astrophysics*, **9**:159.

Ruderman, M. S. and Roberts, B. (2002). The damping of coronal loop oscillations. *Astrophysical Journal*, **577**:475.

Sakurai, T., Ichimoto, K., Raju, K. P., and Singh, J. (2002). Spectroscopic observation of coronal waves. *Solar Physics*, **209**:265.

Scherrer, P. H. *et al* (1995). The solar oscillations investigation - michelson doppler imager. *Solar Physics*, **162**:129.

Schrijver, C. J., Aschwanden, M. J., and Title, A. M. (2002). Transverse oscillations in coronal loops observed with TRACE: I. an overview of events, movies and a discussion of common properties and required conditions. *Solar Physics*, **206**:69.

Schrijver, C. J. *et al* (1999). A new view of the solar outer atmosphere by the Transition Region And Coronal Explorer. *Solar Physics*, **187**:261.

Wang, T. J., Solanki, S. K., Curdt, W., Innes, D. E., and Dammasch, I. E. (2002a). Doppler shift oscillations of hot solar coronal plasma seen by SUMER: a signature of loop oscillations? *Astrophysical Journal Letters*, **574**:L101.

Wang, T. J., Solanki, S. K., Curdt, W., Innes, D. E., and Dammasch, I. E. (2002b). Oscillating hot loops observed by SUMER. In *Proceedings 11th SOHO workshop. From Solar Minimum to Maximum. Ed. A. Wilson. (ESA SP-508; Noordwijk: ESA)*, page 465.

Wang, T. J., Solanki, S. K., Curdt, W., Innes, D. E., and Dammasch, I. E. (2002c). Oscillating hot loops observed by SUMER: examples and statistics. In *Proceedings IAU Colloquium. Magnetic coupling of the solar atmosphere. Ed. H. Sawaya-Lacoste. (ESA SP-505; Noordwijk: ESA)*, page 199.

Wang, T. J., Solanki, S. K., Innes, D. E., Curdt, W., and Dammasch, I. E. (2003). Slow-mode standing waves observed by SUMER in hot coronal loops. *Astronomy and Astrophysics*, **402**:L17.

Wilhelm, K. *et al* (1995). SUMER - solar ultraviolet measurements of emitted radiation. *Solar Physics*, **162**:189.

[1] University of Michigan 'Space science and spacecraft applications',
http://www.windows.ucar.edu/spaceweather/aoss335 quietsun1.html,
accessed February 2003
[2] Yohkoh Public Outreach Project,
http://solar.physics.montana.edu/YPOP/Spotlight/SunInfo/Transregion.html,
accessed September 2002
[3] TRACE website,
http://vestige.lmsal.com/TRACE/POD/TRACEpodoverview.html,
accessed January 2002